

Influence of covariance of aerosol and meteorology on co-located precipitating and non-precipitating clouds over Indo-Gangetic Plains

Nabia Gulistan¹, Khan Alam^{1*}, Yangang Liu²

¹Department of Physics, University of Peshawar, Peshawar, 25120, Pakistan

²Environmental & Climate Science Department, Brookhaven National Laboratory, USA

*Correspondence: Khan Alam (khanalam@uop.edu.pk)

HIGHLIGHTS

- Strong aerosol-cloud relations under unstable meteorological conditions led to the formation of thick precipitating clouds.
- In thick clouds, the activation of cloud droplets is weakly dependent on aerosols.
- Optically thin clouds led to a high precipitation rate.

ABSTRACT

Aerosol-cloud-precipitation-interaction (ACPI) plays a pivotal role in the global and regional water cycle and the earth's energy budget; however, it remains highly uncertain due to the underlying different physical mechanisms. Therefore, this study aims to systematically analyze the effects of aerosols and meteorological factors on ACPI in the co-located precipitating (PCs) and non-precipitating clouds (NPCs) clouds in winter and summer seasons by employing the long-term (2001-2021) retrievals from Moderate Resolution Imaging Spectroradiometer (MODIS), Tropical Rainfall Measuring Mission (TRMM) coupled with the National Center for Environmental Prediction/National Center for Atmospheric Research (NCEP/NCAR) reanalysis-II datasets over the Indo-Gangetic Plains (IGP). The results exhibit a decadal increase in aerosol optical depth (AOD) over Lahore (5.2%), Delhi (9%), Kanpur (10.7%), and Gandhi College (22.7%) and a decrease over Karachi (-1.9%) and Jaipur (-0.5%). The most stable meteorology with high values of lower tropospheric stability (LTS) is found in both seasons over Karachi. In the summer season, the occurrence frequency of clouds is high (74%) over Gandhi College, 60% of which are PCs. Conversely, the least number of PCs are found over Karachi. Similarly, in the winter season, the frequency of cloud occurrence is low over Karachi and high over Lahore and Gandhi College. The analysis of cloud top pressure (CTP) and cloud optical thickness (COT) indicate high values of cloud fraction (CF) for thick and high-level clouds over all study areas except Karachi. The microphysical properties such as cloud effective radius (CER) and cloud droplet number

32 concentration (CDNC) bear high values ($CER > \sim 15 \mu\text{m}$ and $CDNC > \sim 50 \text{ cm}^{-3}$) for both NPCs
33 and PCs in summer. The AOD-CER correlation is good (weak) for PCs (NPCs) in winter. Similarly,
34 the sensitivity value of the first indirect effect (FIE) is high (ranging from 0.2 ± 0.13 to 0.3 ± 0.01
35 in winter, and from 0.19 ± 0.03 to 0.32 ± 0.05 in summer) for PCs and low for NPCs. The
36 sensitivity value for the second indirect effect (SIE) is relatively higher (such as 0.6 ± 0.14 in
37 winter and 0.4 ± 0.04 in summer) than FIE. Sensitivity values of the aerosol-cloud interaction
38 (ACI) are low (i.e., -0.06 ± 0.09) for PCs in summer Furthermore, the precipitation rate (PR)
39 exhibits high values in summer season, primarily due to the significant contribution from optically
40 thick clouds with lower CDNC ($< \sim 50 \text{ cm}^{-3}$) and larger CER, and intermediate contribution from
41 optically thick clouds with higher CDNC ($> \sim 50 \text{ cm}^{-3}$).

42

43 **Keywords:** Aerosol-cloud-precipitation-interaction, Aerosol optical depth, cloud effective radius,
44 cloud droplet number concentration, lower tropospheric stability, relative humidity, first indirect
45 effect, second indirect effect, precipitation sensitivity.

46 1. Introduction

47 The aerosol-cloud-precipitation-interaction (ACPI) and aerosol-radiation-interaction (ARI)
48 significantly influence climates at the regional and global scales (Romero et al., 2021). Assessing
49 the direct and indirect effects of aerosols is crucial to understanding and predicting the energy
50 budget and the water cycle. In the direct effect, the absorption and scattering of solar radiation by
51 aerosols lead to the warming of the atmosphere and cooling of the earth's surface (Zhou et al.,
52 2020), causing changes in the lower tropospheric stability (LTS) that further lead to modulation of
53 precipitating (PCs) and non-precipitation clouds (NPCs) (Andreae & Rosenfeld, 2008).
54 Precipitating clouds are thick clouds with significant vertical development and high moisture
55 content, form under unstable atmospheric conditions, such as cumulonimbus and nimbostratus,
56 that produce precipitation reaching the ground. In contrast, non-precipitating clouds are typically
57 thin, have low moisture content, and form under stable atmospheric conditions, including cloud
58 types like cirrus, cirrostratus, altostratus, and stratus, which generally do not produce significant
59 precipitation (Houze Jr, 2014).

60 In the indirect effect, the water-soluble aerosols such as soil dust, sulfates, nitrates, and other
61 organic aerosols ejected naturally and anthropogenically serve as cloud condensation nuclei (CCN)
62 and ice nucleating particles (INP). Hence, aerosols affect the aerosol-cloud-interaction (ACI) by
63 influencing the growth of cloud droplets and cloud droplet number concentration (CDNC)
64 (Twomey et al., 1977; Albrecht, 1989; Jiang et al., 2002; Chen et al., 2011; Tao et al., 2012). The
65 increase of CDNC and decrease of cloud droplet effective radius (CER) inhibit the onset of
66 precipitation and increase the cloud lifetime (Albrecht, 1989). Conversely, the decrease in CDNC
67 and increase in CER increases the probability of precipitation rate (PR). Conversely, Stevens and
68 Feingold (2009) have shown that initially, more sea salt carried by high wind speed inhibits
69 precipitation formation. However, the same sea spray tends to seed the coalescence by producing
70 larger CER that leads to enhanced precipitation.

71 In the last few decades, most of the cultivable land of the Indo-Gangetic Plain (IGP) has been
72 replaced by urban developments. Due to the fastest growth of population, urbanization,
73 industrialization, and massive combustion of biomass and fossil fuels in residential homes and
74 factories, a decadal increase in aerosols is observed over IGP. The high aerosol loading may affect
75 the formation of tropospheric clouds and seasonal precipitation patterns (Kaskaoutis et al., 2011;
76 Singh et al., 2015; Thomas et al., 2021). The high aerosol loading makes IGP suitable for the study
77 of ACPI. Besides, frequent variations in cloud fraction (CF), extreme precipitation and drought
78 abrupt temperature changes (e.g., heat waves), and irregular unseasonal rains may cause major and
79 unavoidable hazards at local and regional levels in the future (Zhou et al., 2020).

80 In the last two decades, the scientific community has focused on quantification of ACI using both
81 observations (Feingold et al., 2003; Koren et al., 2004; Costantino et al., 2010; Wang et al., 2015;
82 Zhao et al., 2018, Guo et al., 2019; 2020; Anwar et al., 2022) and modeling techniques (Chen et
83 al., 2016, 2018; Wang et al. 2020; Zhou et al., 2020; Sharma et al., 2023). Although, a similar
84 recent study (Anwar et al., 2022) attempted to understand the sensitivities of ACI and the first
85 indirect effect of different subsets of AOD to the different conditions of RH and wind directions
86 and found a decrease (increase) in CER with aerosol loading Twomey effect (anti-Twomey effect)
87 over the monsoon (weak and moderately intensive monsoon) regions. However, the above study
88 excluded the other significant meteorological parameters such as LTS, PR, and T_{850} and was also
89 limited to the monsoon regions of Pakistan only. Further, in the context of warm rain processes, it

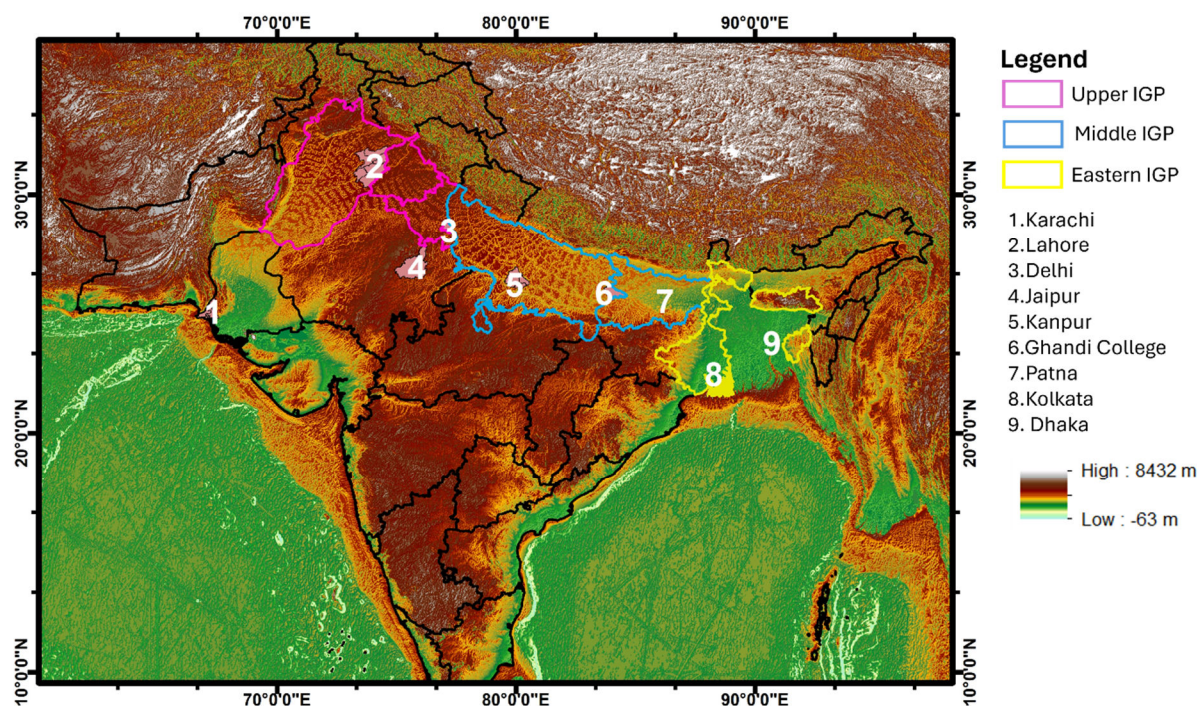
90 is generally understood that the high concentration of aerosols capable of serving as CCN leads to
91 enhanced CDNC known as the first indirect effect (FIE) or Twomey effect (Twomey et al., 1977).
92 It is also widely acknowledged that CDNC plays a pivotal role in cloud microphysics and
93 significantly influences the onset of precipitation and retention of water in clouds called the second
94 indirect effect (SIE) (Gryspeerd et al., 2016; Naud et al., 2017). Whilst, in the above study, the
95 analysis of CDNC is also not addressed. Therefore, the present study aims to deepen the previous
96 study (Anwar et al., 2022), by a long-term and detailed analysis of the ACPI including aerosol-
97 indirect effects for low-level liquid clouds extended over the whole IGP for understanding different
98 mechanisms (condensation, droplet growth and precipitation rate) of cloud and precipitation
99 formation. Due to the absence of in-situ measurement facilities and the constraints of limited
100 computational resources, the study concentrated on satellite data for specific locations across the entire IGP.
101 These locations were strategically chosen due to their positioning within significant aerosol belts, where
102 the concentration and behavior of aerosols are of particular interest. Therefore, the satellite-based approach
103 was chosen as it provides detailed insights into aerosol dynamics in these critical regions while also
104 benefiting from the broader spatial coverage of satellite data.

105 This study is focused on estimating the variations in sensitivities of aerosol-cloud relationship to
106 the variations in aerosol loading at specified meteorological conditions for low-level PCs and
107 NPCs in the summer and winter seasons over the IGP. This study is unique in using a large number
108 of samples, classification of liquid clouds in PCs and NPCs, further classification of clouds in low,
109 mid, and high-level clouds through joint COT-CTP histograms, quantification of the sensitivities
110 of FIE, SIE, total indirect effect (TIE), and ACI to CDNC. The significant meteorological
111 parameters considered include temperature at 850 hPa, LTS, relative humidity (RH%) at 850 hPa,
112 vertical velocity (ω), and PR. Furthermore, by utilizing the Moderate Resolution Imaging
113 Spectroradiometer (MODIS) and Tropical Rainfall Measuring Mission (TRMM) data, the
114 correlation of cloud microphysical properties (CER and CDNC) and AOD at specified values of
115 LTS and cloud liquid water path (CLWP) is examined, and precipitation sensitivity at constant
116 macro-physical condition is estimated.

117 **2. Study area and methodology**

118 **2.1. Study area**

119 The selected study area (Fig. 1) comprises the upper, middle, and eastern portions of the IGP. The
120 upper part consists of the densely populated and developed regions of the eastern part of Pakistan
121 i.e., Karachi (24.87°N, 67.03°E) and Lahore (31.54°N, 74.32°E) whereas the middle part comprises
122 the northern part of India i.e., Delhi (28.59°N, 77.22°E), Kanpur (26.51°N, 80.23°E), Jaipur
123 (26.91°N, 75.81°E), Gandhi College (25.87°N, 84.13°E), Kolkata (22.57°N, 88.36°E), Dhaka
124 (23.80°N, 90.41°E) and Patna (25.59°N, 85.13°E). The data analysis for the eastern part of IGP
125 (Kolkata, Dhaka, and Patna) is documented as supplementary materials.



126
127 **Figure 1.** Topography of the study area.

128 **2.2. Methodology**

129 **2.2.1. MODIS, NCEP/NCAR reanalysis-II and TRMM data**

130 Moderate Resolution Imaging Spectroradiometer (MODIS) is a major constituent of NASA's Earth
131 Observing System (EOS). MODIS is orbiting with two onboard satellites, Terra and Aqua,
132 launched in 1999 and 2002 respectively, with a range of 2330 km spanning the entire globe in a
133 day. It provides data and information with a spatial resolution of 1° to study atmospheric processes

134 and physical structure (Kedia et al., 2014; Srivastava et al., 2015). This study uses the daily mean
 135 of combined dark target and deep blue AOD at 0.55 μm , cloud top pressure (CTP), cloud top
 136 temperature (CTT), CF, CER, and COT for liquid clouds from level 3 aerosol-cloud data product
 137 MOD08-TERRA. Data with AOD > 1.5 are excluded to avoid potential misidentification of
 138 aerosols as clouds. The following adiabatic approximation (Brennguier et al., 2000; Wood, 2006;
 139 Kubar et al., 2009; Michibata et al., 2014) is used to calculate CDNC (cm^{-3}):

$$140 \quad \text{CDNC} = \left(\frac{B}{\text{CER}} \right)^3 * \sqrt[3]{2 * \text{CLWP} * \gamma_{\text{eff}}}$$

141 (1)

142 Where $B = \sqrt[3]{\left(\frac{3}{4}\pi\rho_{\text{water}}\right)} = 0.0620$, ρ_{water} is the liquid water density, γ_{eff} is the adiabatic
 143 gradient of liquid water content in the moist air column (Wood, 2006). Value of γ_{eff} range from 1
 144 to 2.5×10^{-3} at a temperature of 32 K to 104 K (Brennguier, 1991; Zhu et al., 2018; Zhou et al.,
 145 2020). The CLWP is estimated by use of

$$146 \quad \text{CLWP} = \frac{5\rho_w(\text{CER})(\text{COT})_w}{9},$$

147 (2)

148 Where, ρ_w is the water density at room temperature (Koike et al., 2016).

149 National Center for Environmental Prediction/National Center for Atmospheric Research
 150 (NCEP/NCAR) reanalysis datasets provide global reanalysis data sets that combine satellite
 151 observations with the simulation of models through data assimilation (Purdy et al., 2016). Daily
 152 data for meteorological parameters including temperature, RH%, and ω at 850 hPa are retrieved at
 153 a spatial resolution of T62 Gaussian grid ($1.915^\circ \times 1.875^\circ$) from NCEP reanalysis-II datasets, and
 154 used to calculate lower tropospheric stability (LTS) defined as (Li et al., 2017):

$$155 \quad \text{LTS} = \theta_{700} - \theta_{1000}$$

156 (3)

157 where θ is the potential temperature and the subscripts denote the pressure levels of 700
 158 hPa and 1000 hPa.

159 The Tropical Rainfall Measuring Mission (TRMM) is the first Joint satellite mission between
 160 NASA America and National Space Development Agency (NASDA) Japan, utilizing the visible
 161 infrared and microwaves to measure the rain precipitation over tropical and subtropical regions.
 162 The main TRMM instruments that are used to measure rain precipitation are precipitation radar
 163 (PR) and TRMM Microwave Imager (TMI). Where PR is operating at a frequency of 13.8 GHz
 164 and TMI is a passive microwave radiometer consisting of nine channels. A calibrated data set
 165 TRMM-2B31 of TRMM Combined Instrument (TCI) for TRMM Multi-Satellite Precipitation
 166 Analysis (TMPA) is formed from an algorithm that uses TMI and PR. The product TMPA 3B42
 167 gives the rain precipitation averages on a daily and sub-daily basis. In the current study, the data
 168 product TMPA or TRMM 3B42 is used for the retrieval of PR daily. The spatial resolution of
 169 TRMM 3B42 is $0.25^\circ \times 0.25^\circ$ and is available from the year 1998 to till date.

170 2.2.2. Methodology

171 The present study is designed to analyze and quantify the ACPI for PCs and NPCs in winter and
 172 summer under a variety of meteorological conditions. The daily mean data of each parameter for
 173 warm clouds are retrieved from the respective satellites and NCEP/NCAR reanalysis-II for each
 174 study site. Subsequently, the VLOOKUP function in Microsoft Excel is applied to filtering out
 175 counts where data is not available, searching for values of a parameter in the first column, and
 176 retrieving the values of other parameters in the same rows on the corresponding dates in a large
 177 dataset. The data are then segregated into two subsets for the summer and winter seasons. Based
 178 on precipitation data from TRMM, the subsets are further divided into precipitating and non-
 179 precipitating clouds.

180 The sensitivities of cloud parameters to CDNC are analyzed through the following formulation
 181 considered from previous studies (Zhou et al., 2020):

$$182 \frac{d\ln(COT)}{d\ln(CDNC)} = -\frac{d\ln(CER)}{d\ln(CDNC)} + \frac{d\ln(CLWP)}{d\ln(CDNC)} \quad (4)$$

183 In this study, the term on the left side of equation (3) is defined as total indirect aerosol effect
 184 (TIE), and the first and second terms on the right side of the equation are defined as the first indirect
 185 aerosol effect (FIE), *and second indirect effect (SIE), respectively*. Similarly, the sensitivity
 186 of CDNC to AOD is evaluated by employing the index of ACI:

187
$$ACI_{CDNC} = \frac{dln(CDNC)}{dln(AOD)} \quad (5)$$

188 The sensitivity of PR to CDNC is calculated from the following equation (Jung et al., 2012) :

189
$$S_0 = \left(- \frac{\partial ln(PR)}{\partial ln(CDNC)} \right)_{COT} \quad (6)$$

190 **3. Results and Discussion**

191 3.1. Regional and seasonal distribution of AOD

192 AOD is a commonly used proxy for aerosol concentration in the atmosphere and is analyzed here
193 (Fig. 2-3).

194 IGP characteristically exhibits a diverse and massive pool of aerosols due to its unique topography.
195 The western part of IGP is a coastal location and inlet for the westerly winds. Therefore, dry
196 regions and the Arabian Sea in the west contribute dust, sea salt, and water vapors to the region.
197 The Himalayas in the north act as barriers to the winds, leading to the trapping of aerosols over
198 the central part of IGP. Therefore, this region exhibits a high concentration of anthropogenic
199 aerosols. The Bay of Bengal in the east allows southeasterly winds to enter passing across Dhaka,
200 Kolkata, and Patna to Delhi and Lahore (Hassan et al., 2002; Anwar et al., 2022). The westerly
201 and easterly winds traverse forested hilly terrain, rivers, and lakes elevating humidity levels and
202 initiating the cloud formation by activation of the newly originated small aerosol particles as CCNs
203 and cloud formation affecting the local microclimate.

204 Fig. 2 shows a decadal variation in time average maps for combined dark target and deep blue
205 AOD retrieved at 0.55 μm over the entire study area for the years (2001-2010) and (2011-2021).
206 Also, Table 1 illustrates the percentage change in decadal averaged values of AOD. The results
207 indicate that AOD exhibits a decrease over Karachi (-1.9%) and Jaipur (-0.5%). An increase in
208 AOD is observed over Lahore (5.2%), Delhi (9%), Kanpur (10.7%) and Gandhi College (22.7%).
209 Similarly, Table 1S shows the decadal change in AOD over Kolkata (18%), Dhaka (22.6%), and
210 Patna (23.3%). Similar to Gandhi College, an increase is observed over all three areas. Reasons
211 for the increase of aerosols include multiple sources of aerosols, human behavior, socio-economic

212 development at local and regional levels, and unique topography for the persistence and retaining
213 of aerosols.

214 Fig.3(a-b) shows the probability density function (PDF) for AOD, illustrating different
215 distributions in the summer and winter seasons. Fig.3a shows that the distribution of AOD over
216 Delhi, Kanpur, and Gandhi College is similar. However, a shift in the peak value of PDF towards
217 high values of AOD over Lahore and low values over Jaipur illustrate comparatively high and low
218 aerosol concentration in the summer season over Lahore and Jaipur respectively. Likewise, Fig.
219 1S shows the seasonal PDF values of AOD over Kolkata, Dhaka, and Patna. The results indicate
220 similar seasonal distribution functions over all three areas of eastern IGP. In both seasons PDF
221 peaks for high values of AOD are observed over Patna showing a high concentration of aerosols
222 as compared to Kolkata and Dhaka.

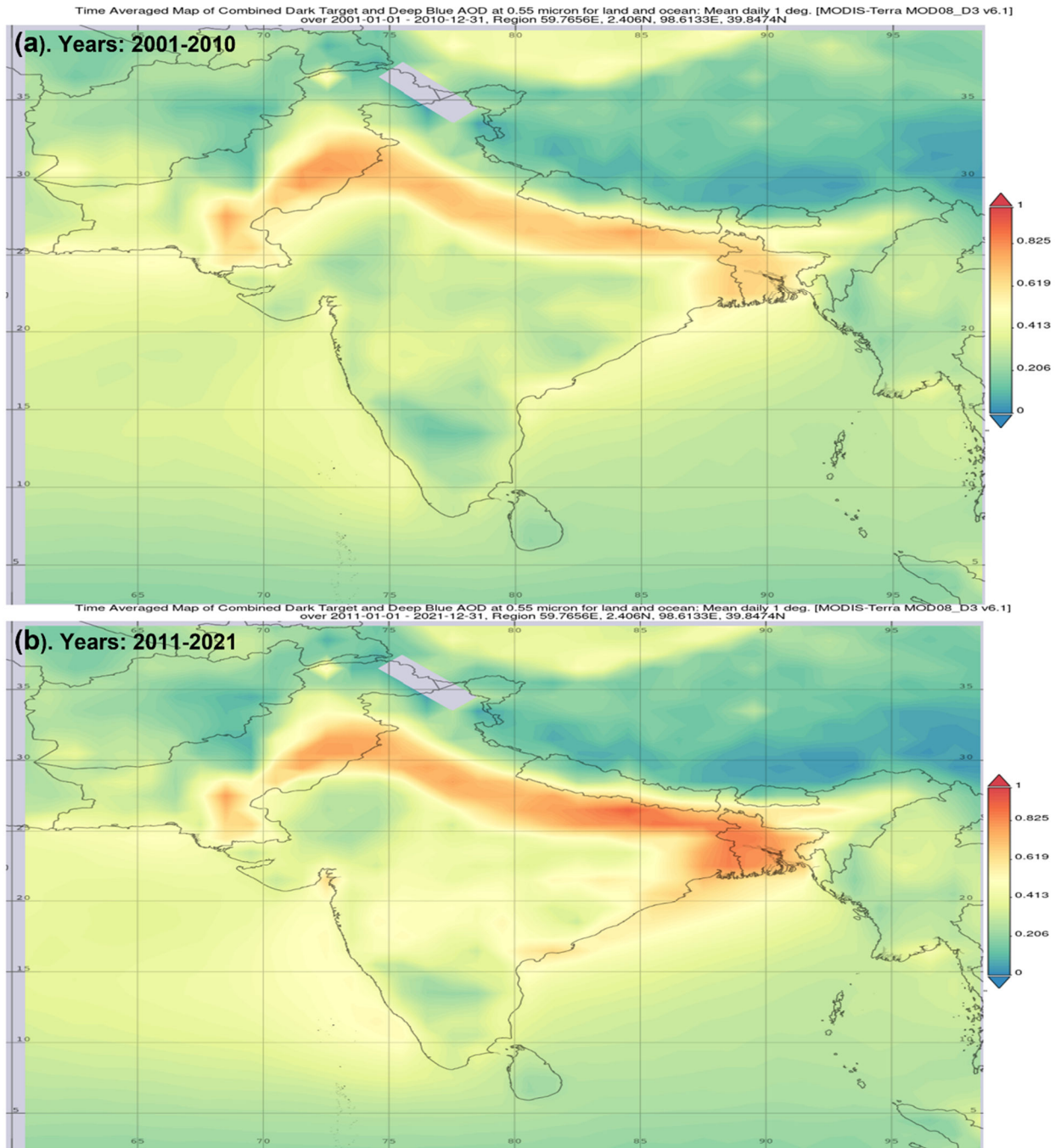
223 The loading of high concentrations of aerosols is owing to the high density of population,
224 industrialization, and human activities. The major sources of aerosols in all months of the year
225 include vehicular emission originating from old transport facilities, emission of smoke and soot
226 during consumption of biomass for cooking, heavy industrial emission, and aerosols produced in
227 seasonal harvesting and crop residue burning. All these sources produce organic aerosols which
228 are characterized as hydrophilic particles and have the potential to act as CCN. Likewise, the soil
229 dust particles also act as good CCN due to their hygroscopic nature (Sun & Ariya, 2006).
230 Moreover, the meteorological conditions also play a substantial role in enhancing AOD values
231 such as the uplifting of loose soil dust and swelling of aerosols due to holding the water vapors
232 (wv) for a long time (Masmoudi et al., 2003; Alam et al., 2010; Alam et al., 2011;). Also, the lower
233 but flat PDF curve demonstrates low values of AOD over Karachi. Ali et al., 2020 associated the
234 low AOD values over Karachi with the westerly and southwesterly wind currents at tropospheric
235 level. However, the decreasing trend in AOD over the coastal city may also be attributed to the
236 variations in other meteorological parameters like T and RH.

237 As compared to the summer season, the pattern of PDF in winter is significantly different as shown
238 in Fig. 3b. The low value of PDF (0.5) for the high value of AOD (0.9) over Karachi illustrates a
239 comparatively pristine atmosphere. Similarly, the PDF peaks for Lahore, Delhi, and Jaipur (0.7,
240 0.7, and 0.8) indicate comparatively high AOD over Delhi. Likewise, the distribution over Kanpur
241 and Gandhi College similarly illustrates similar values of AOD (1.1 and 1.2 respectively). These

242 high values of AOD are attributed to the high emission of anthropogenic aerosols at local and
243 regional levels over the central part of IGP (Delhi, Jaipur, Kanpur and Gandhi College).

244 Few authors attributed the reduced values of AOD in the winter season to the wet scavenging and
245 suppressed emission of aerosols from the earth surface (Alam et al., 2010; Zeb et al., 2019).

246 However, in our case, the low (high) values in winter (summer) are associated with the dispersion
247 of fine (course) mode particles due to the variations in meteorological conditions.



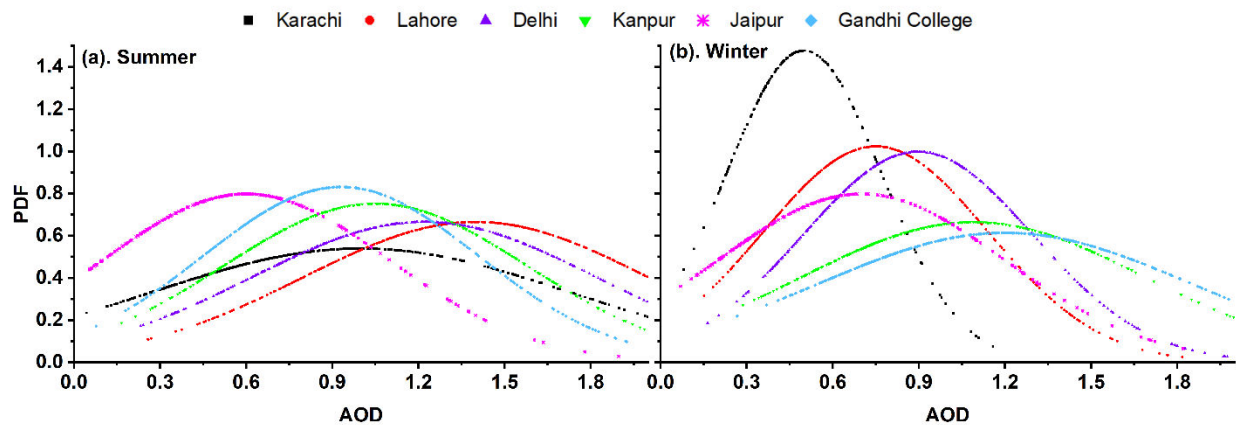
248
 249
 250
 251
 252
 253

Figure 2. Decadal increase (year: 2001-2010 and 2011-2021) in AOD over study sites.

254 **Table 1.** Decadal percentage variations in average values of AOD over all study areas

	Karachi	Lahore	Delhi	Kanpur	Jaipur	Gandhi College
Total number of counts	5902	6171	5823	5201	5907	5125
Decadal change in AOD	-1.9%	5.2%	9%	10.7%	-0.5%	22.7%

255



256

257 **Figure 3.** The probability density function (PDF) of AOD over study sites is shown (a) and (b) for the summer and
 258 winter seasons respectively.

259 **3.2. Climatology of meteorological parameters**

260 Generally, LTS has relationships to factors such as temperature, humidity, wind patterns, and
 261 atmospheric pressure over extended periods. It is also widely acknowledged that atmospheric
 262 stability, temperature, RH wind speed, and direction play a significant role in cloud formation
 263 (Yang et al., 2015; Tao et al., 2012). Therefore, the influence of long-term variations in the said
 264 meteorological parameters is considered in the current study. The variations in meteorological
 265 parameters have an unavoidable impact on ACPI. The parameters considered in this study include
 266 the temperature, LTS to determine the lower atmospheric stability and instability that influence the
 267 process of cloud and precipitation formation through its significant implications on evaporation
 268 and convection of the air parcel, the RH% to estimate the level of wv and the ω to assess the
 269 suitable atmospheric dynamics. Fig.4 shows the variations in LTS values for NPCs and PCs in the
 270 winter and summer seasons. In the winter season, the LTS values are high for NPCs and
 271 comparatively lower for PCs over entire study areas. In the summer season, the scenario is reversed
 272 with high values for PCs but low values for NPCs, suggesting a stable tropospheric layer on rainy

273 days. This stabilization may be attributed to the cold pools generated by the evaporation of falling
274 rain droplets (Wu et al., 2017). The lower LTS values for NPCs in the summer season suggest the
275 likelihood of stronger instability that causes a high potential for vertical motion and the
276 development of thunderstorms. However, Karachi exhibits a distinct pattern of LTS with the
277 highest values in each case, which indicates the existence of the most stable tropospheric layer in
278 Karachi due likely to moist and cold sea breeze due to the city's coastal location.

279 The median values computed for the remaining meteorological parameters considered in this study
280 are listed in Table 2. The high values in each case are indicated in bold and the low values are
281 italicized. The results show that in the winter season, the temperature at 850 hPa (T_{850}) is relatively
282 high for NPCs ranging from 281 K to 285.6 K. The increase in RH% for PCs during winter ranged
283 from (59.5)% to (71.5)%. Also, the $\omega > 0$ for NPCs and < 0 for PCs in the winter season.

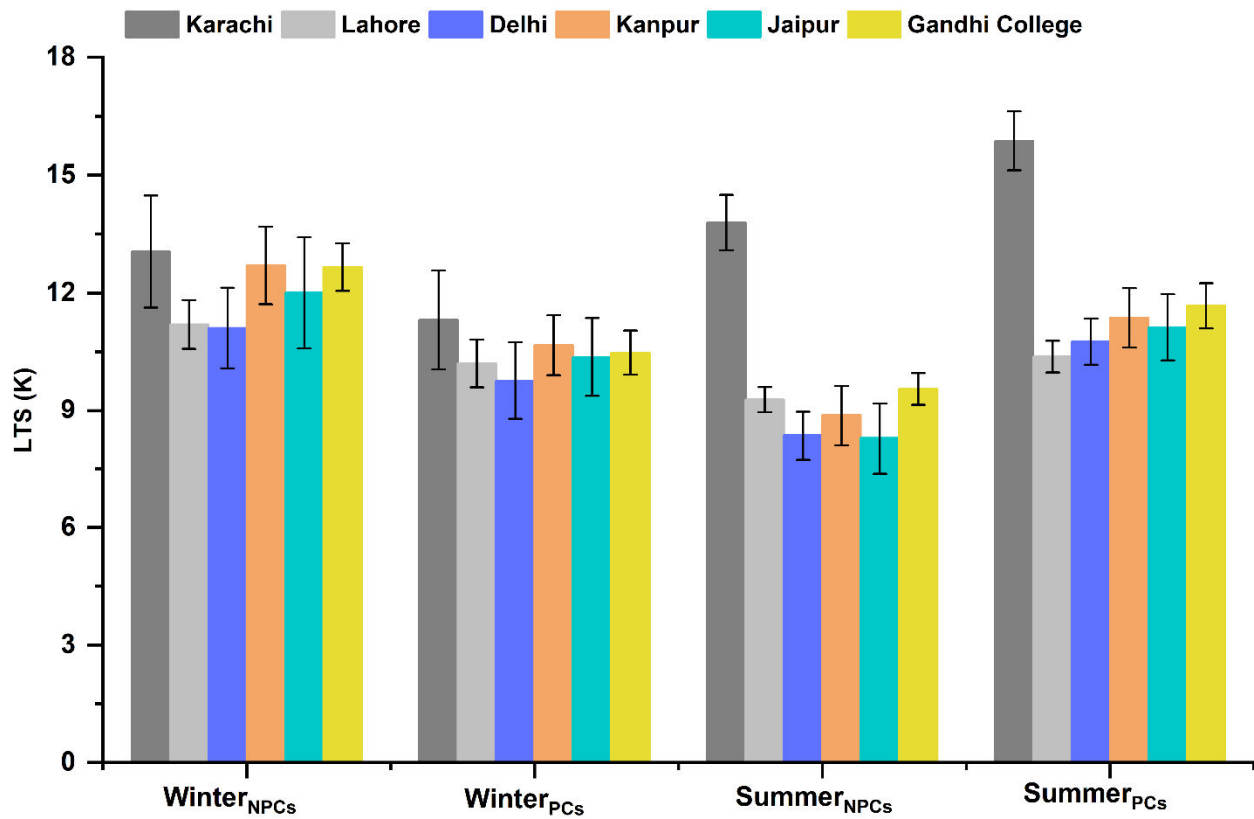
284 In the summer season, it is observed that T_{850} is comparatively higher than that for the winter
285 clouds and ranges from 298.3 to 300.2 K and 296.5 to 298.3 K for NPCs and PCs respectively.
286 The high values of T_{850} are due to intense solar fluxes in the summer season that keep the
287 temperature of the earth's surface and adjacent atmospheric layer higher. Also, the increase in
288 RH% during summer ranged between 33.5-51.7 % for NPCs. The reason for the high values of wv
289 and RH% is mainly the suitable thermodynamical conditions such as evaporation and convection
290 due to the high temperature of the earth's surface and air (Sherwood et al., 2010). The results show
291 high values of RH% 70.1% (85%) in the winter (summer) season for PCs over Gandhi College.
292 Conversely, notable fluctuations in RH% are observed over the coastal city, of Karachi, with values
293 of 71.5% (65.9%) in winter (summer). Similarly, Fig. 2S and Table 2S show the LTS conditions
294 for PCs and NPCs. The high LTS values indicate more stable conditions over Dhaka. Similarly,
295 Table 2S shows the seasonal average values for other meteorological parameters. The results
296 indicate high values of T_{850} , RH%, and ω 295.5 (297.5) K, 88.8 (83.5)%, and -0.19 (-0.17) m/s
297 respectively for PCs (NPCs) for over Patna in summer.

298 Besides, during the last two decades, the wv and fog over the Arabian Sea increased (Verma et al.,
299 2022). Therefore, the high values of wv and RH% in summer months are due to the high-speed
300 zonal winds that blow in the summer season and transport water vapors and sea salt from the
301 surface of the Arabian Sea and hydrophilic aerosols such as soil dust from deserts of Iran, Pakistan,
302 and India to IGP. Moreover, during the winter season, elevated humidity levels are noticeable over

303 IGP, particularly in the vicinity of Gandhi College. This increased humidity is a result of
 304 evapotranspiration driven by agricultural practices, irrigation, the presence of rivers and lakes, and
 305 the introduction of moist, cold air from western winds (Nair et al., 2020). Where $\omega < 0$ for PCs
 306 over all study areas except Karachi.

307 The distinct variations in meteorological parameters reveal the occurrence of clouds with diverse
 308 properties. The detailed analysis of such clouds is given in the next subsections.

309



310

311 **Figure 4.** Variations in lower tropospheric stability (LTS) over all study sites for PCs and NPCs in winter and summer
 312 seasons, the error bars show the standard deviation (SD) values.

313 **Table 2.** Median values of meteorological parameters for PCs(NPCs) in summer and winter seasons. Maximum values are for both types of
 314 clouds shown in bold and minimum values are indicated in italics.

	Winter Season			Summer Season		
	T ₈₅₀ (K)	RH%	ω (m/s)	T ₈₅₀ (K)	RH%	ω (m/s)
Karachi	284.6 (285.8)	71.5 (38)	-0.038 (<i>0.030</i>)	295.9 (298.8)	65.9 (45.9)	<i>0.005</i> (-0.003)
Lahore	280.5 (<i>281.2</i>)	59.5 (35.5)	-0.02 (0.065)	298.3 (300.2)	65 (33.5)	-0.028 (<i>0.025</i>)
Delhi	284.2 (283.1)	60.2 (33.8)	-0.1 (0.04)	296.5 (299.4)	64.2 (42)	-0.05 (<i>-0.001</i>)
Kanpur	283.8 (284.1)	65.7 (36)	-0.1 (0.048)	296.5 (298.4)	73.7 (43.6)	-0.13 (<i>-0.08</i>)
Jaipur	283.9 (284.1)	66 (40.5)	-0.065 (0.049)	296.8 (298.7)	64 (51.7)	-0.04 (<i>-0.029</i>)
Gandhi College	283.2 (284.1)	70.1 (45.7)	-0.1 (0.05)	296.9 (298.3)	85 (42.5)	-0.16 (<i>-0.11</i>)

315

316

317

318

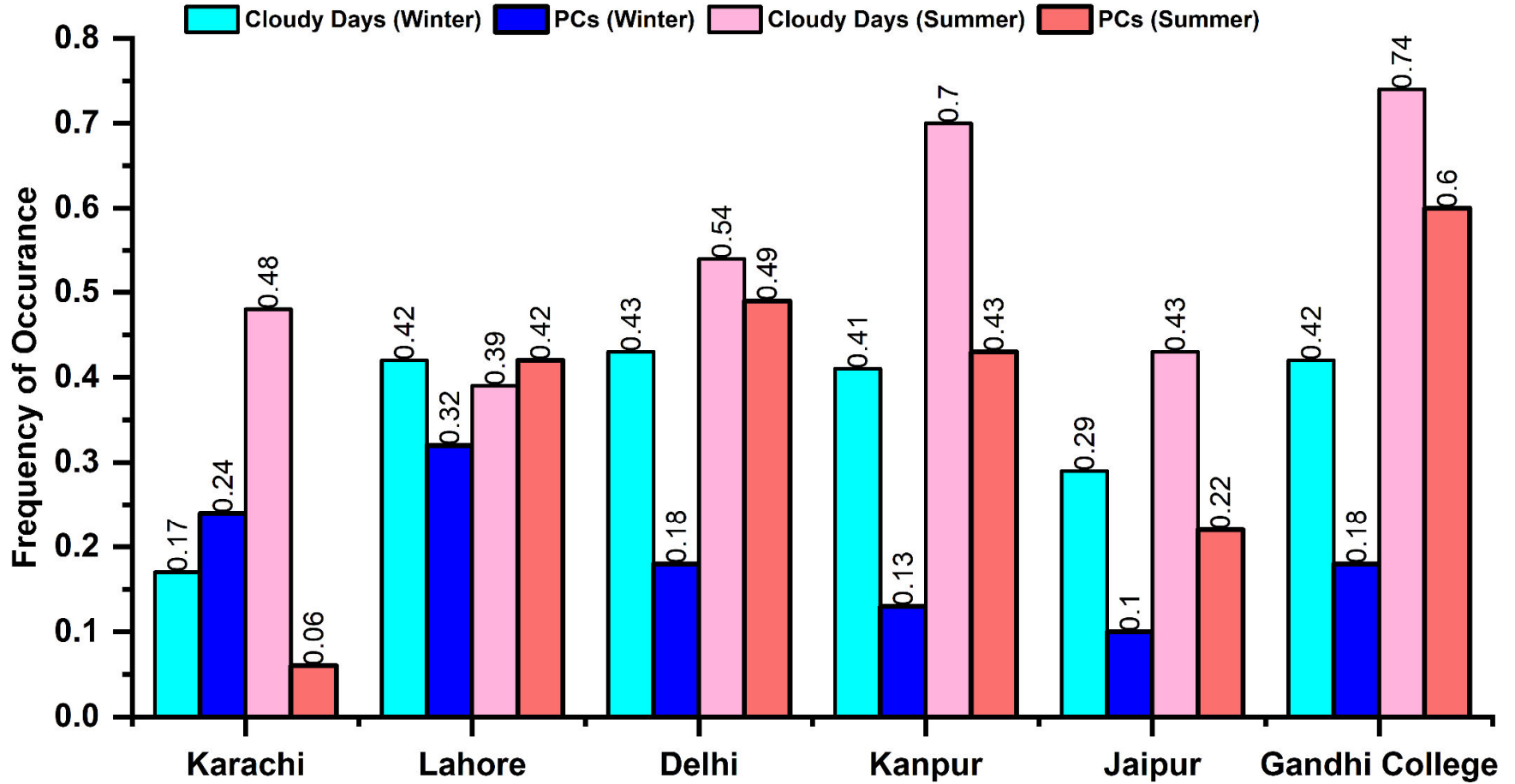
319

3.3. Regional and seasonal distribution of clouds and precipitations

3.3.1. Regional and seasonal differences in cloud occurrence and its microphysical structure

Fig.5 shows the frequency of occurrence of precipitable clouds and the total number of cloudy days. Chen et al. (2018) suggested the COT to be an effective measure for assessing the clouds and potential for precipitation. In our case, to avoid any overestimation, the COT data are aligned with PR data on corresponding dates and then filtered to include $COT \sim > 5$ for PCs. The results show that in the winter season, the frequency of clouds is low over Karachi and high over Lahore and Gandhi College. The results suggest the high number of PCs only over Lahore. In the summer season, a high number i.e., 74 % of the total data counts over Gandhi College are identified as cloudy days, 60 % of which are PCs. Similarly, most of the clouds over Lahore, Delhi, and Jaipur are PCs. Conversely, the least number of PCs (6 %) are found over Karachi. Likewise, Fig. 3S shows the total number of cloudy days and the number of days on which PCs occurred. The high occurrence of clouds is observed over Kolkata 83% (60%) and Dhaka 91% (69%) in the summer (winter) season. The high occurrence of PCs in summer is due likely to the significant impact of elevated aerosols with the southwesterly winds on the summer monsoons and the occurrence of PCs. Therefore, Kolkata and Dhaka are of critical importance from the perspective of aerosol loading and ACI (Dahal et al., 2022).

338



340

341

Figure 5. The frequency of occurrence of total cloudy days (including PCs and NPCs) and only PCs is shown for both winter and summer seasons.

342 Table 3 shows the criteria adopted from previous papers (Rossow & Schiffer, 1999; Wyant et
343 al., 2006; Sharma et al., 2023) for further classification of NPCs and PCs into different types
344 of clouds. The aim of identifying the cloud types is to assess the cloud regimes and their vertical
345 structure for a better understanding of ACPI. Following table 3, Fig. 6 shows joint histograms
346 of COT-CTP displaying the median values of CF for nine different types of clouds. For a quick
347 visual comparison, the cloud types are ordered from low to high-level clouds. Also, for each
348 histogram, the bins of COT and CTP are located on the x- and y-axis respectively. The CF of
349 each bin is represented with the colored bar with its value mentioned in the histograms as shown
350 in Fig. 6.

351 The results exhibit noticeable differences in the pattern of cloud regimes over all study areas.
352 The diverse CF values are observed in the winter and summer seasons for NPCs and PCs over
353 Karachi. In the winter season, only stratus NPCs ($23 < \text{COT} < 60$, $800 > \text{CTP} > 680$ hPa) are
354 dominant with $\text{CF} \sim 0.9$. While, in summers, the high value of $\text{CF} \sim 0.9$ for low and
355 intermediate thickness of high-level clouds such as Cirr-Stratus NPCs ($3.6 < \text{COT} < 23$, $180 <$
356 $\text{CTP} < 440$ hPa) are observed. Similarly, the types of PCs in both summer and winter seasons
357 that occurred with $\text{CF} \sim 1.0$ include cirrus and cirrus-stratus. The relatively reduced value of CF
358 for thick NPCs in winter and PCs in summer is attributed to the low values of AOD and high
359 values of LTS. The results depicted slight differences and similarities in CF values for thick
360 and thin NPCs respectively in the winter season for all areas except Karachi. Besides, the high-
361 level PCs are identified in the two bins of CTP ($180 < \text{CTP} < 440$ hPa) and ($440 < \text{CTP} < 680$
362 hPa) over all study areas. The formation of these similar types of PCs in winter is associated
363 with the similarities in ω , LTS values, and aerosol concentration.

364 Likewise, in the summer season, the matrices of PCs and NPCs exhibit a wide range of cloud
365 types. However, the CF values are comparatively high for PCs. Most of the identified PCs are
366 formed in the two bins of CTP ($180 < \text{CTP} < 440$ hPa) and ($440 < \text{CTP} < 680$ hPa) with CF
367 values ranging from 0.8 to 1.0. The results suggest low values of CF for the low-lying thick
368 NPCs over all study areas. Moreover, the results illustrate a more frequent occurrence of all
369 three types of thick NPCs in one bin of COT ($23 < \text{COT} < 60$) and all the three types of high-
370 level NPCs for CTP ($180 < \text{CTP} < 440$ hPa) over Delhi, Kanpur, and Gandhi College.
371 Therefore, these are considered the cloudiest regimes. Besides, contrasting regional variations
372 are also observed in PCs. The maximum CF values for all types of PCs are observed over
373 Kanpur and Gandhi College. Similarly, relatively good values of CF in a bin of COT ($23 <$

374 COT < 60) and a bin of CTP (180 < CTP < 440 hPa) over Lahore, Delhi, and Jaipur depict the
 375 frequent occurrence of thick and high-level PCs respectively. In addition, among all the
 376 estimated low-level PCs, cumulus and strato-cumulus exhibit good CF values (0.7) over
 377 Kanpur and Gandhi College. The formation of thick clouds can be attributed to the enhanced
 378 convection process due to atmospheric instability.

379
 380

Table 3. Classification of clouds based on CTP – COT joint histograms.

CTP (hPa)	COT		
	0-3.6	3.6-23	23 to >60
440 to <180	Cirrus	Cirr-Stratus	Deep convection
680-440	Alto-Cumulus	Alto-Stratus	Nimbo-Stratus
<800 to 680	Cumulus	Strato-Cumulus	Stratus

381

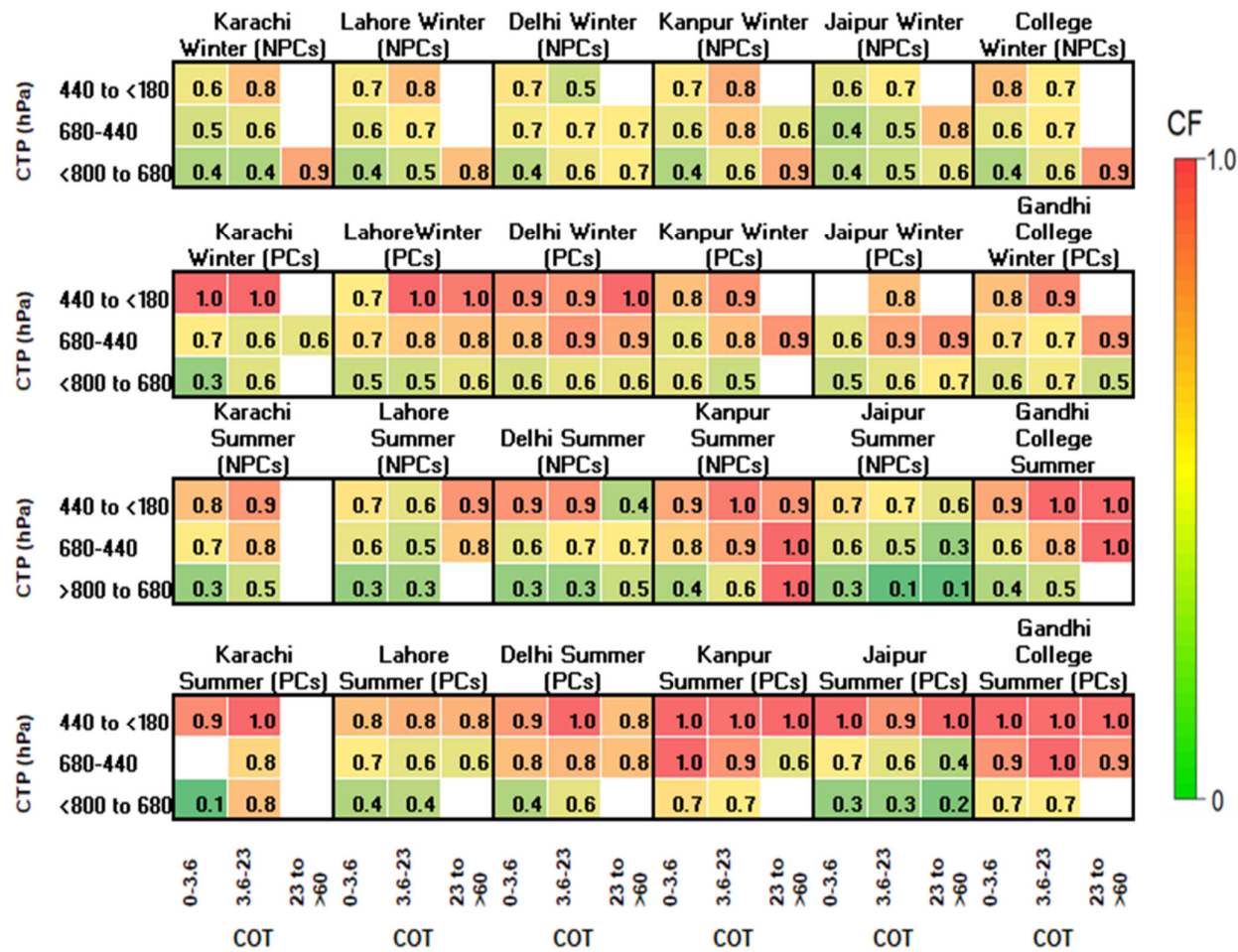


Figure 6. Types of NPCs and PCs in winter and summer season

382

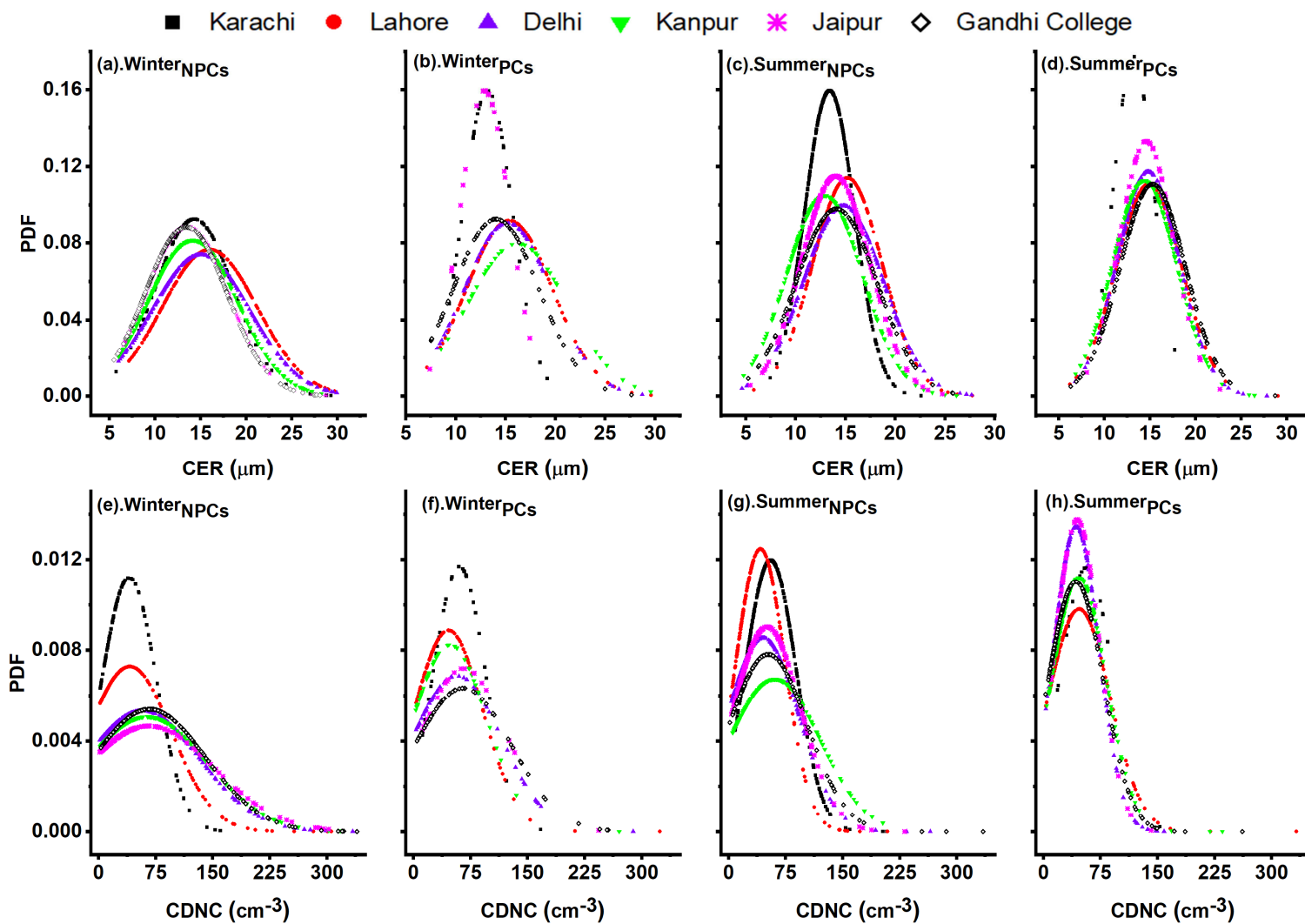
383

384 After estimating the cloud types, Fig. 7 shows the probability distribution function (PDF) of
385 cloud microphysical properties for the identification of differences in the microstructure of
386 NPCs and PCs in the summer and winter seasons. From the results, it is depicted an
387 approximately similar pattern for the CER of NPCs in winter. However, the clouds have high
388 peaks of PDF for lower values of CDNC over Karachi. The low number of CDNC results in
389 thin NPCs as shown in Fig.7. Similarly, Fig. 7(c and g) shows the microstructure of NPCs in
390 summer. The results indicate that as compared to CER values in winter, the probability of CER
391 $> \sim 15 \mu\text{m}$ is high in the summer season. However, the high peak for CER $< 15 \mu\text{m}$ is observed
392 over Karachi. Similarly, the CDNC shows a high probability for CDNC $> 50 \text{cm}^{-3}$ with high
393 PDF values over Karachi. Where the lowest number of CDNC is observed over Lahore
394 indicating the formation of high-level thin NPCs in summer.

395 Fig. 7(b and f) shows the distribution pattern of CER and CDNC of PCs in the winter season.
396 It is observed that the distribution of CER for PCs is like that for NPCs in the winter season.
397 However, PDFs have peak values for relatively higher CDNC, which illustrates the occurrence
398 of thick clouds. Fig. 7(d and h) shows the variations in CER and CDNC in the summer season.
399 The results show a wider distribution for CER $> \sim 15 \mu\text{m}$ and higher peaks for CDNC $> \sim 50$
400 cm^{-3} suggesting the formation of thick PCs in summer as shown in Fig.6.

401

402



403

404

Figure 7. Probability density function (PDF) of precipitating (PCs) and non-precipitating clouds (NPCs) in the winter and summer season

405 **3.4. Aerosol-Cloud-Precipitation Interaction (ACPI)**

406 In the following sections, ACPI is analyzed and discussed in detail for PCs and NPCs in the
407 summer and winter seasons.

408 *3.4.1. Aerosol effects on cloud properties*

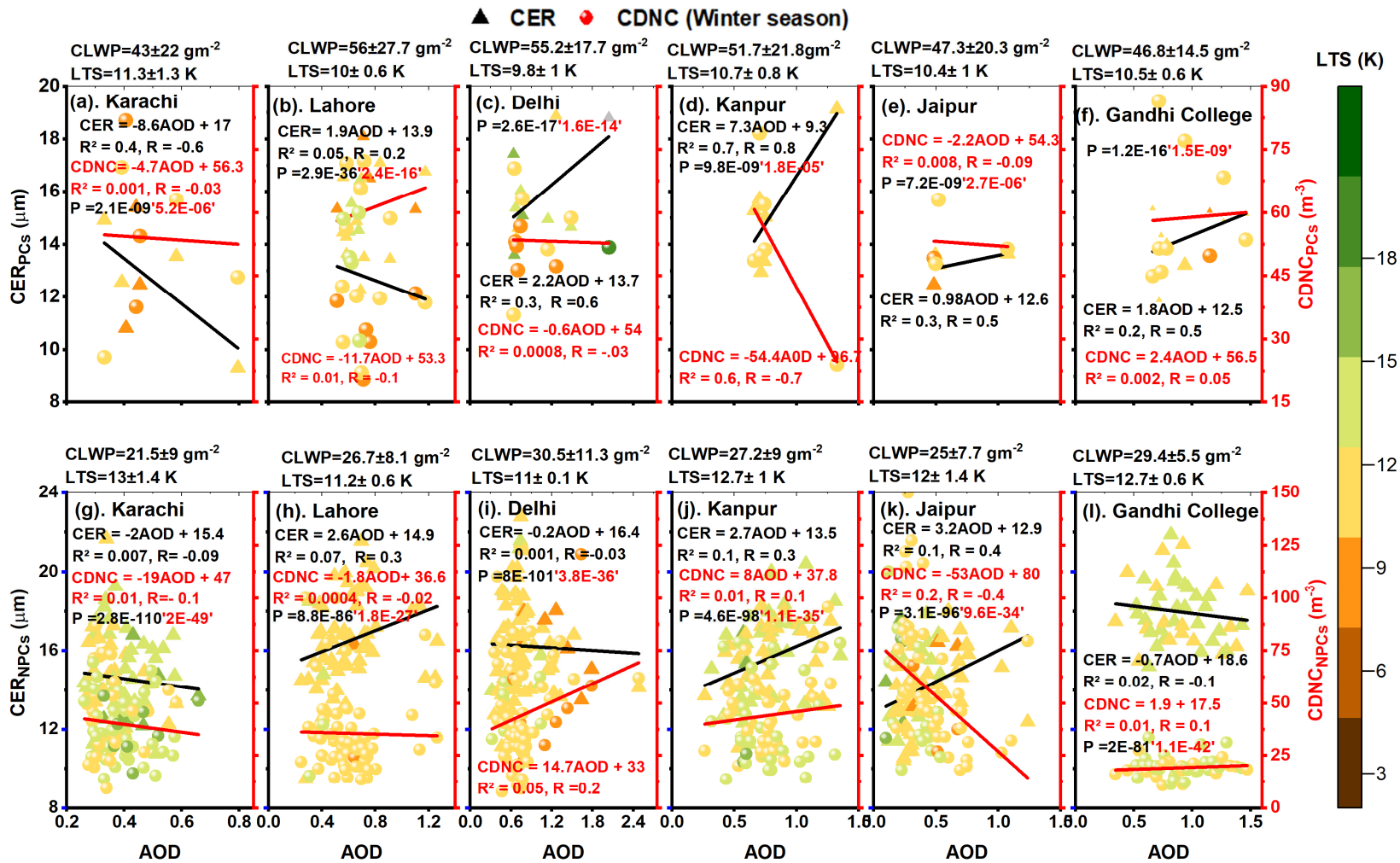
409 The impact of aerosols on CDNC and CER of PCs and NPCs is illustrated as scatter plots in
410 Fig. 8-9. The quantification of the AOD-CER and AOD-CDNC relationships is demonstrated
411 through detailed linear regressed slopes, regression coefficients (R^2), and Pearson's correlation
412 coefficient (R). The color bar represents the variations in LTS. The results show that the two-
413 sample student's t-test is carried out to analyze the AOD-CER and AOD-CDNC relationship in
414 view of statistics. The results illustrate that the relationships are statistically significant at a
415 95% ($p < 0.05$) significance level for all study areas. Fig.8 shows that in the winter season, the
416 AOD-CER correlation is good for PCs and weak for NPCs. The results also show that the LTS
417 values are higher for NPCs. The weak AOD-CER correlation may be linked to the inhibition
418 of droplet growth due to less soluble aerosols, originating from biomass burning (Kang et al.,
419 2015). In our case, all the selected study areas are among the most urbanized and industrialized
420 areas of IGP. Therefore, most of the prevailing aerosols are the less soluble soot and BC
421 particles. That weakened activation of cloud droplets inhibits the formation of PCs and
422 evaporates to higher altitudes thereby increasing the droplet residence time (Kumar & Physics,
423 2013). Besides, the results show a contrasting pattern of LTS values. Although RH over Karachi
424 ($38.3 \pm 9\%$) is higher than over the other study areas (shown in Table 2), the negative AOD-
425 CER correlation is observed over Karachi due to its coastal location, the low value of AOD and
426 high level of LTS.

427 Fig. 9 illustrates the AOD-CER and AOD-CDNC correlation in the summer season. The results
428 depict a more significant and positive AOD-CER correlation in the summer season than winter
429 season. Unlike the winter season, high LTS values are observed for PCs. Yuan(2008)
430 associated the positive AOD-CER correlation with the soluble organic aerosols. Myhre et al.
431 (2007) hypothesized that the positive AOD-CER correlation is a maximum for low CTP and a
432 minimum for high CTP. Hence, in our study, referring to the approximated CF values shown
433 in Fig.6, the significant and positive AOD-CER correlation under unstable atmospheric
434 conditions resulted in thick and high-level clouds. Furthermore, it is observed that CER and
435 CDNC values for NPCs increase with increasing instability. Meanwhile, the enhanced process
436 of droplet activation may result in large AOD, higher CER, giant, and fewer CCN (Yuan, 2008).

437 Therefore, the weak correlation of AOD with CER and CDNC may be due to the
438 anthropogenically ejected water-soluble organic aerosols and a smaller number of CCN.

439 Fig. 5S and 6S show the impact of AOD on CER and CDNC for PCs and NPCs in winter and
440 summer respectively. The results indicate a positive and weak AOD-CER correlation of 0.2,
441 0.07, and 0.004 for NPCs over Kolkata, Dhaka, and Patna respectively, and for PCs (0.08) over
442 both Kolkata and Patna. Similarly, a positive and weak AOD-CDNC is observed over all areas
443 for PCs. Likewise, Fig. 6S also illustrates weak AOD-CER correlation is 0.06, 0.2, and 0.12
444 for both types of clouds in summer. As compared to other areas, the correlation analysis is less
445 significant over Karachi, Kolkata, Dhaka, and Patna. This can be attributed to the persistence
446 of diverse aerosol types influenced by their coastal locations, different meteorology, and the
447 alternating inflow and outflow of easterly and westerly winds.

448 Recent advances in remote sensing led to cost-effective solutions and an increase in available
449 data at various temporal and spatial resolutions to bridge scientific gaps among different
450 disciplines. While satellite-based retrievals have many advantages over in-situ and ground-
451 based measurement such as broader regional coverage and enhanced spatial resolution, they
452 are still prone to considerable uncertainties owing to the indirect nature of remote-sensing,
453 retrieval algorithms, thermal radiance, infrequency of satellite overpasses, and cloud top
454 reflectance (Hong et al., 2006; Tian et al., 2010; Hossain et al., 2006). In our study, apart from
455 the aforementioned factors contributing to the uncertainty, any residual cloud contamination
456 could also lead to biased retrieval of AOD. Likewise, satellite-based retrievals for cloud
457 properties are crucial to understanding the pivotal role of clouds in climate and the role of
458 clouds is still a dominant source of uncertainty in the prediction of climate change. These,
459 uncertainties in AOD and retrievals of cloud properties also propagate through the modeling
460 process, potentially leading to less accurate climate predictions. Likewise, these uncertainties
461 appeared to influence the findings in the current investigation. For instance, a limited
462 correlation between AOD and CER is observed over Lahore, particularly in cloudier regimes
463 as depicted in Fig. (5-6). This contrasts with robust impacts documented in earlier studies
464 (Michibata et al., 2014). However, high sensitivity of SIE is observed for PCs particularly in
465 the winter season indicating the delay in the onset of precipitation and more retention of clouds.



466

467

468

Figure 8. AOD-CER and AOD-CDNC regression and correlation coefficient considered at 95% confidence level for PCs and NPCs over all study areas in the winter season.

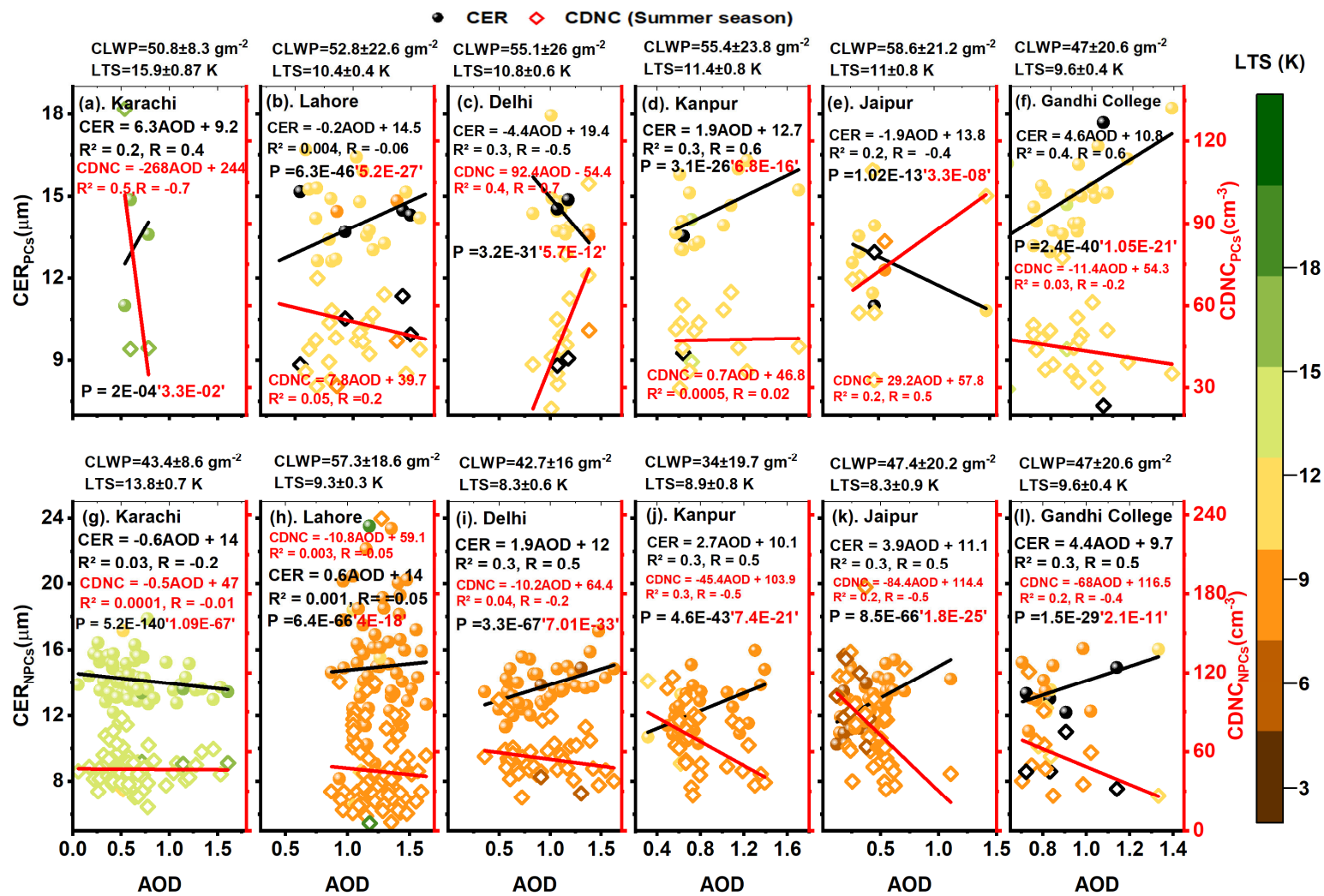


Figure 9. Same as Fig. 8 but in the summer season.

469

470

3.4.2. Seasonal variations in sensitivities of aerosol-cloud indirect effects and ACI

471 Fig.10 shows an assessment of four ACI sensitivities in terms of CDNC using daily mean
472 values of MODIS observations available over the entire study area. Studying the effects of
473 aerosols on the co-located clouds is a challenging task due to the overestimation of thin clouds
474 in AOD retrievals. Therefore, to minimize the propagation of AOD retrieval errors in ACI, the
475 current study attempted to estimate the sensitivities of different cloud mechanisms to CDNC.
476

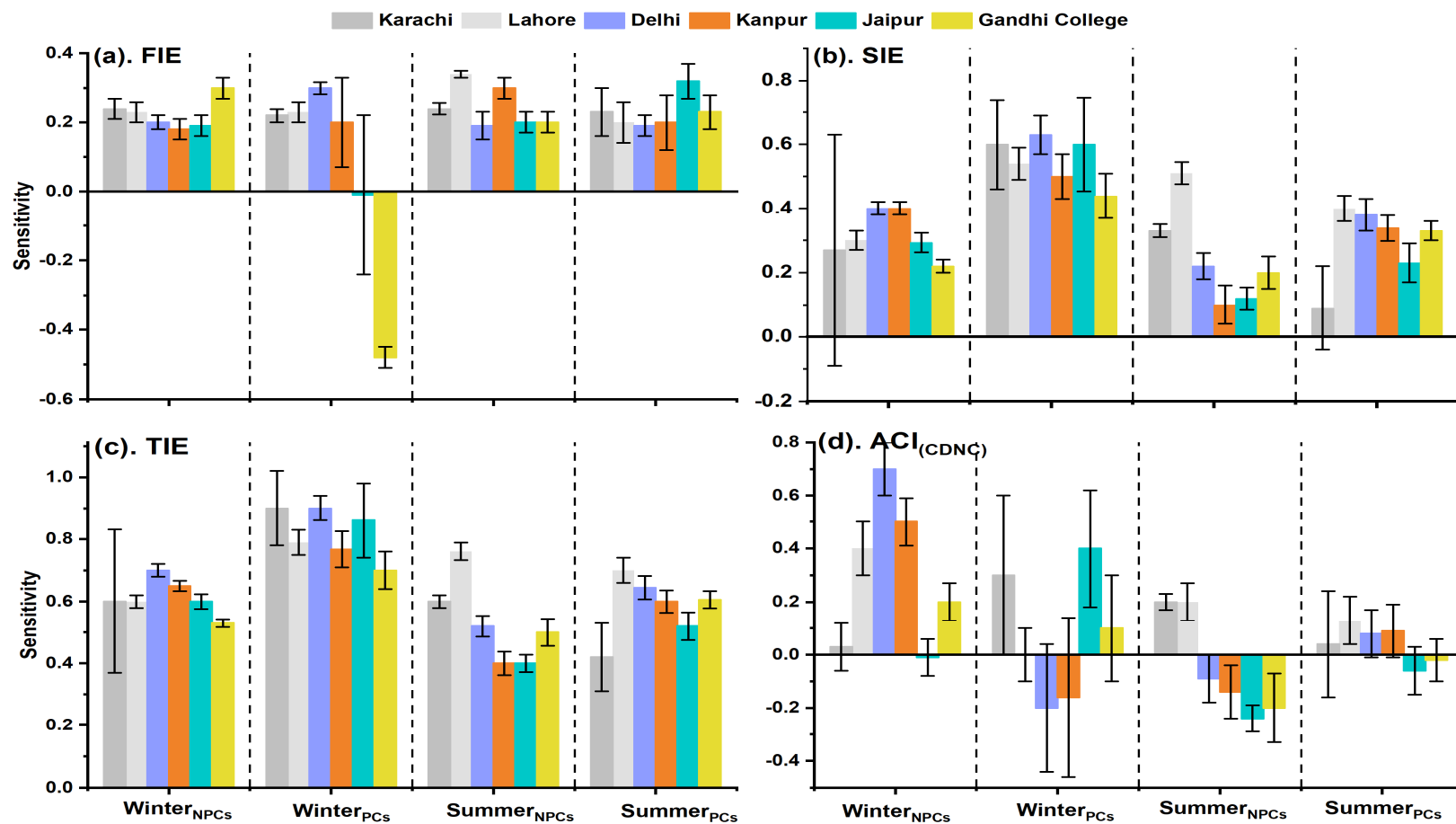
477 The sensitivity of CER to CDNC is assessed as a signature of FIE as shown in Fig.10a. The
478 positive values illustrate that CER decreases with an increase in CDNC revealing the
479 occurrence of the Twomey effect. While the negative values depict the anti-Twomey effect.
480 Tripathi et al., (2007) divided IGP into four regions western, central, eastern part of IGP, and
481 the foothills of the Himalayas. Their results depicted a high concentration of dust in the western
482 part, and an increase in anthropogenic aerosols as one moves from the western to the eastern
483 part of IGP. Therefore, they attributed the resulting strong indirect effect in winter to the high
484 concentration of regional anthropogenic pollution. However, in our case, the FIE is investigated
485 for both PCs and NPCs in both seasons. The resulting approximations in the winter season
486 show strong (weak) sensitivity of FIE for PCs (NPCs). Similarly, the estimated sensitivity of
487 FIE for all NPCs and PCs is also positive in the summer season. Fig. 7S(a) shows sensitivities
488 for FIE in both seasons for PCs and NPCs. The results indicate high values of sensitivity FIE
489 in the winter season which is similar to the results for Karachi, Lahore, Delhi, and Kanpur as
490 shown in Fig. 10 a. This is attributed to high levels of aerosol emission from residential heating
491 and industrial activities. Furthermore, the results illustrate higher values of FIE in summer. This
492 is attributed to the massive aerosol loading due to aerosol carried by winds and originating
493 from anthropogenic activities and unstable meteorology.

494 Fig. 10b illustrates the sensitivity of CLWP to CDNC as a proxy for the evaluation of the SIE
495 or lifetime effect. The positive sensitivity estimated for all NPCs and PCs suggested that the
496 CLWP increases with an increase in aerosol. Further, the results show that the sensitivity of
497 SIE is stronger for PCs in winter which indicates the delay in the onset of high PR. Similarly,
498 the results show that the SIE sensitivity values are higher for PCs than for NPCs in the
499 corresponding seasons. Therefore, the results depict that the lifetime of PCs is greater than
500 NPCs. This is attributed to the high level of RH for PCs as shown in Table 2. Fig. 10 (a and b)
501 shows that the FIE sensitivities are weaker than SIE.

502 Fig. 10c shows the TIE in terms of the sensitivity of COT to CDNC. The results illustrate
503 positive values of sensitivity for all NPCs and PCs which indicate that COT increases with an
504 increase in aerosol concentration. The results also reveal that the sensitivity of TIE is a linear
505 sum of the sensitivities of FIE and SIE. Further, the results also suggest that the variations in
506 TIE sensitivity are largely dependent on SIE.

507 Fig.10d shows the sensitivity of CDNC to AOD as an estimation of ACI in terms of CDNC.
508 The positive values show the increase in CDNC with the increase in AOD. Therefore, positive
509 ACI reflects the inhibition of precipitation formation. Whilst, the negative values illustrate the
510 decrease in CDNC and enhanced PR (Fan et al., 2018). The results depicted relatively large
511 and positive sensitivities for NPCs in winter over Lahore, Delhi, and Kanpur, which inhibits
512 the onset of rainfall. The Sensitivity of ACI for NPCs in summer is positive over Karachi and
513 Lahore and negative over Delhi, Kanpur, Jaipur, and Gandhi College. Ackerman et al. (2004)
514 associated the negative ACI_{CDNC} with the wet scavenging and mixing of air by entrainment.
515 In our case, negative ACI may be due to the growth of CER and a decrease in CDNC with
516 aerosol loading under unstable conditions (shown in Fig. 9). Further, the magnitude of
517 sensitivity for PCs in summer is low. This can be due to the droplet growth through collision
518 coalescence and wet scavenging in thick clouds, decreased dependency on CCN.

519



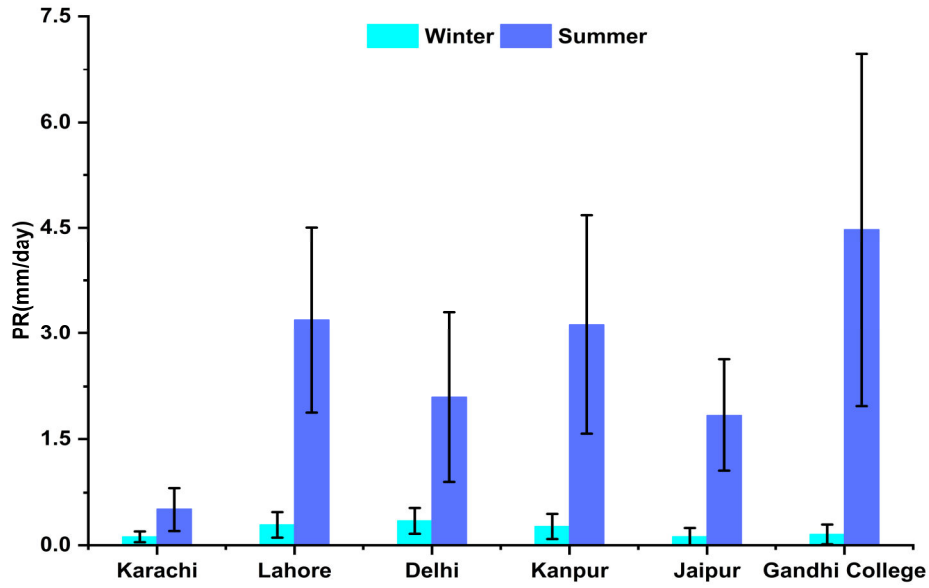
521

522 **Fig. 10.** The sensitivity matrices estimated for an aerosol-cloud relationship using CDNC are shown in (a) $FIE = -\left(\frac{\partial \ln(CER)}{\partial \ln(CDNC)}\right)$ (b) $SIE = \left(\frac{\partial \ln(cLWP)}{\partial \ln(CDNC)}\right)$,
 523 (c) $TIE = \left(\frac{\partial \ln(COT)}{\partial \ln(CDNC)}\right)$ and (d) $ACI = \left(\frac{\partial \ln(CDNC)}{\partial \ln(AOD)}\right)$. Where the error bars show the standard deviation (SD).

524 3.4.3. *Aerosol effects on precipitation*

525 Fig. 11 shows the average values of PR in mm/day retrieved from TRMM. The results show
526 an obvious seasonal difference in precipitation occurrence. The reason for the high (low) PR
527 values is due to the suitable meteorological conditions including high (low) LTS values for PCs
528 in the summer (winter) season (shown in Fig. 8-9). The stable atmospheric condition with a
529 high LTS value in winter serves to inhibit the convection process and have a significant impact
530 on controlling the PR in winter (Zhao et al., 2006). Conversely, during the summer season,
531 meteorological instability prevails with low LTS values which result in high RH. This not only
532 causes enhanced AOD due to the water uptake and results in swelled hydrophilic aerosols
533 (Alam et al., 2010; Alam et al., 2011) but also affects the cloud and precipitation formation due
534 to the enhanced evaporation and convection. Additionally, Fig. 8-9 also shows evidently and
535 specifically during summer that the possible cause of positive AOD-CER correlation is the
536 negative AOD-CDNC correlation under unstable meteorology over all areas except Karachi.
537 As a result, Fig. 11 shows high (low) values of PR over all areas with a maximum over Gandhi
538 College (Karachi). The results show a high (low) approximation of PR over Gandhi College
539 (Karachi). Knowing that the rate of conversion of CDNC to precipitation is proportional to
540 CER (Wolf & Toon, 2014). Therefore, the high PR values are due to the growth of bigger cloud
541 droplets in summer. Further, apart from the reasons mentioned in the preceding sections, the
542 other justification for the differently perturbed aerosols, clouds, and precipitation pattern over
543 the study areas in summer is due to the entrance of southeast winds from the Bay of Bengal
544 passing across Gandhi College to Delhi and Lahore and the entrance of same winds from
545 Arabian sea to Pakistan through Karachi (Anwar et al., 2022).

546 Fig. 12 shows scatter plots of PR versus CDNC. The plot is colored with COT to examine the
547 impact of CDNC on PR for similar macrophysics. When CDNC is less, then the COTs are
548 sparse grow larger, form less reflective clouds, and precipitate faster (Kump & Pollard, 2008).
549 The same phenomenon seems true in our case. The results illustrate high PR (0.0007 mm/day)
550 values for clouds with COT ranging from 3 to 28 with $CDNC < \sim 50 \text{ cm}^{-3}$ and intermediate for
551 optically thick clouds and $CDNC > \sim 50 \text{ cm}^{-3}$ in both seasons.

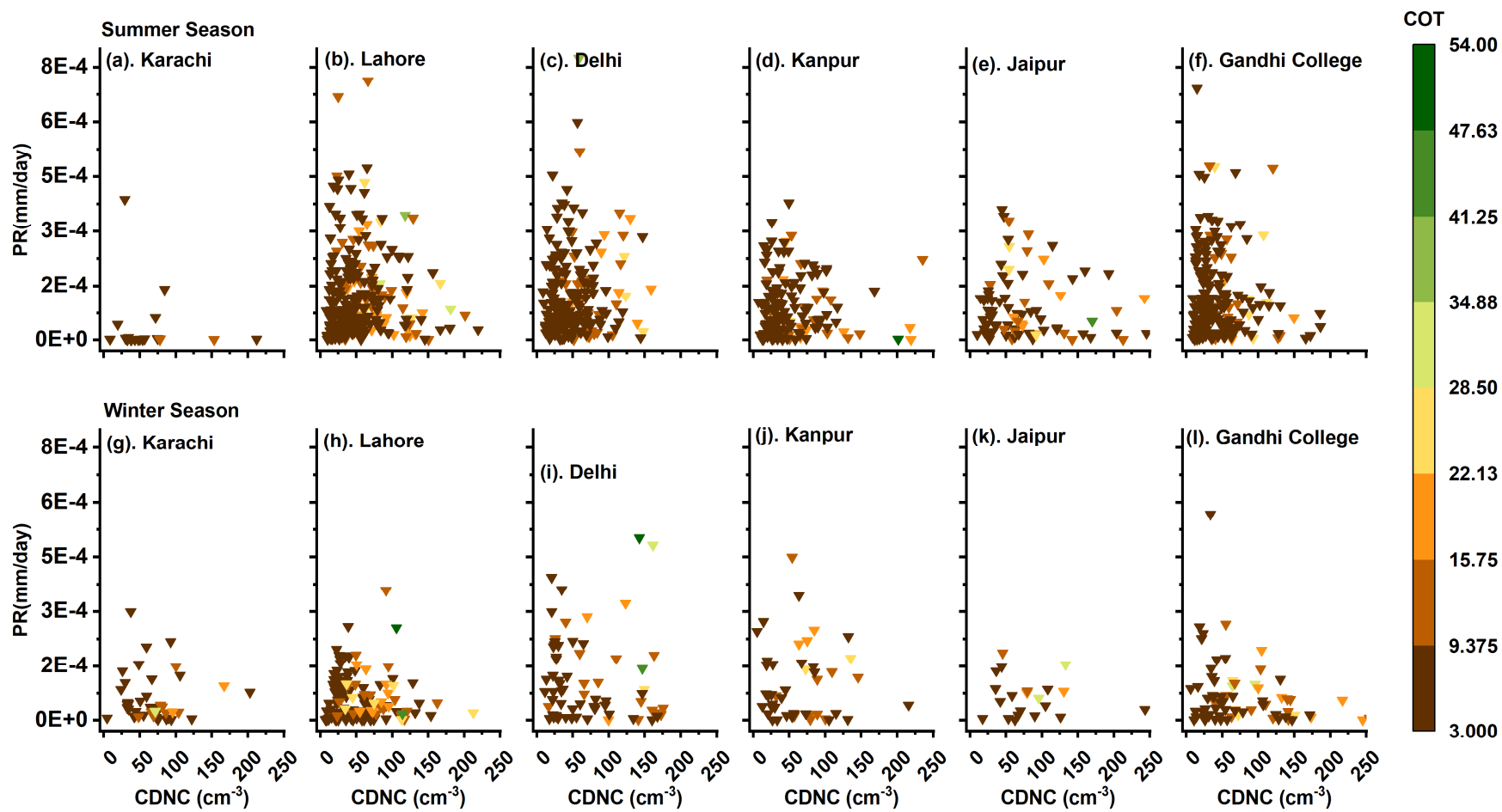


552

553

554

Figure 11. Mean Precipitation rate (PR) for the PCs in winter and summer season and SD values with a 95% confidence interval.



555

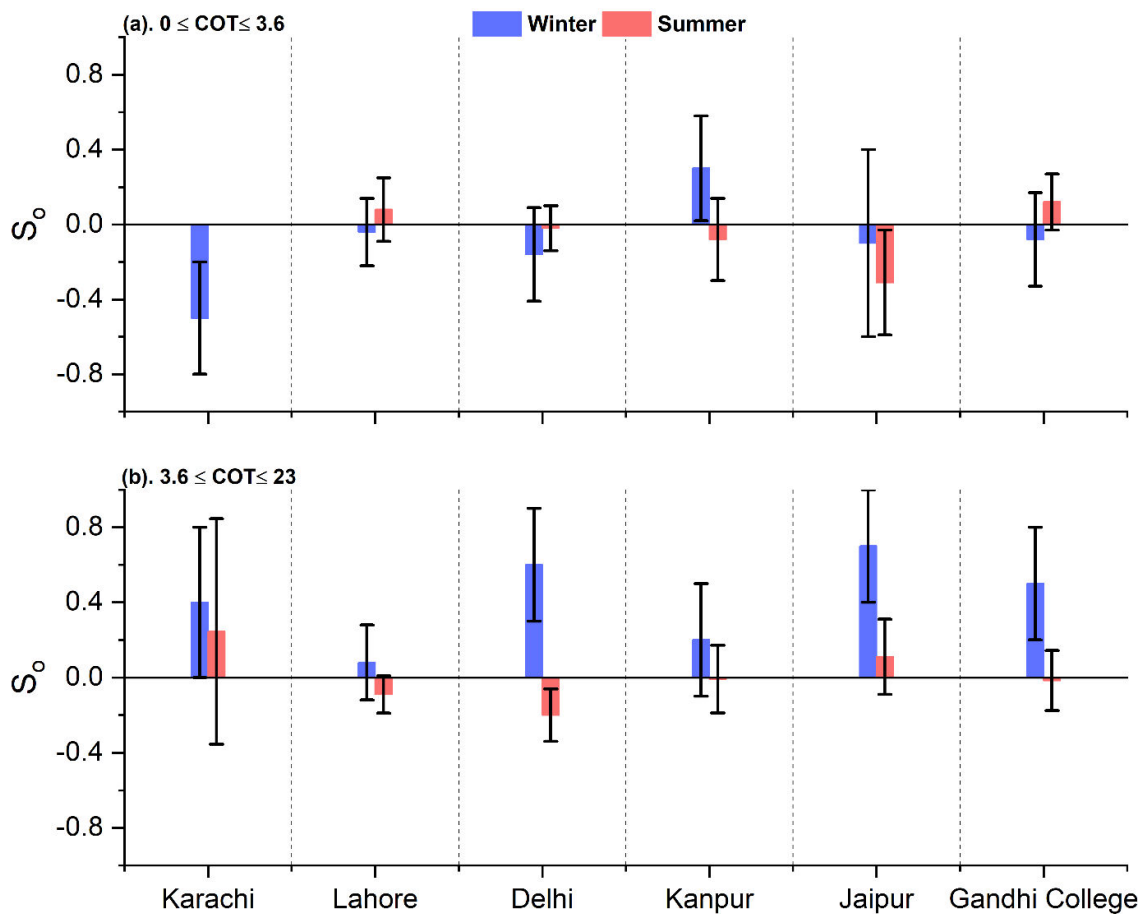
556

557

Figure 12. Scatter diagrams of PR (mm/day) versus CDNC (cm⁻³) in summer and winter seasons. color coding shows the COT of PCs.

558 Fig.13 shows the sensitivity (S_o) of PR to CDNC defined by $S_o = \left(-\frac{dln(PR)}{dln(CDNC)}\right)_{COT}$ for clouds
 559 of low and intermediate thickness illustrated in Fig. 13 a and Fig. 13 b respectively. However,
 560 sensitivity analysis for $COT > 23$ could not be performed due to the smaller number (0 to 04)
 561 of available samples. In the sensitivity equation, the minus sign shows the suppression of
 562 precipitation formation due to the increase in CDNC. Further, when S_o is positive, the
 563 correlation between PR and CDNC is negative; however, for negative S_o , PR and CDNC are
 564 positively correlated. The results show peak values of S_o i.e., 0.7 ± 0.3 , 0.6 ± 0.3 , 0.5 ± 0.3 , and
 565 0.4 ± 0.4 over Jaipur, Delhi, Gandhi College, and Karachi respectively at intermediate values
 566 of COT in winter, indicating the occurrence of lightly precipitating clouds. Referable to Fig.
 567 13b, the low magnitude of S_o 0.2 ± 0.3 and 0.08 ± 0.2 over Kanpur and Lahore respectively is
 568 due to coagulation, in which precipitations are less sensitive to CDNC.

569



570

571 **Figure 13.** The sensitivity ' S_o ' of precipitation rate (PR) for two bins of COT is shown in (a).
 572 $0 \leq COT \leq 3.6$ and (b). $3.6 \leq COT \leq 23$.

573

574 4. Conclusion

575 In this study, the long-term (2001-2021) data retrievals from MODIS coupled with TRMM and
576 NCEP/NCAR reanalysis-II datasets over the entire study area are compiled and analyzed for
577 PCs and NPCs in the winter and summer season. The following are the main findings of this
578 study.

579 A decadal decrease in AOD is observed over Karachi (-1.9%) and Jaipur (-0.5%). Meanwhile,
580 AOD exhibits an increase over Lahore (5.2%), Delhi (9%), Kanpur (10.7%) and Gandhi
581 College (22.7%). The LTS values are High (low) for NPCs (PCs) in winter and for PCs (NPCs)
582 in the summer season. However, among all study areas, Karachi exhibits comparatively high
583 LTS values in both seasons. Apart, the increase in RH% for PCs ranged from 33-57% in winter
584 and from 25-45 % in summer. $\omega > 0$ for all NPCs in winter and < 0 for PCs in both winter and
585 summer seasons.

586 In the winter season, a low frequency of cloudy days over Karachi and a high over Lahore and
587 Gandhi College is estimated. Also, the high number of PCs is estimated only over Lahore. In
588 the summer season, out of the 74 % of the cloudy days, 60 % are PCs over Gandhi College.
589 Similarly, most of the clouds over Lahore, Delhi, and Jaipur are PCs. Conversely, the lowest
590 number of PCs (6 %) is found over Karachi. The high-level PCs are identified in one bin of
591 CTP ($180 < \text{CTP} < 440$ hPa) over all study areas in winter. In the summer season, all three
592 types of high-level and thick PCs have significant values of CF. The low-level PCs are
593 identified as stratus clouds. Further, PDF values for $\text{CER} > \sim 15 \mu\text{m}$ and $\text{CDNC} > \sim 50 \text{cm}^{-3}$
594 for NPCs and PCs are high (low) in summer (winter) over all areas except Karachi.

595 The AOD-CER correlation is good for PCs and weak for NPCs in the winter season. Also, the
596 CER and CDNC values increase with the increase in LTS. The sensitivity value of FIE is high
597 (low) for PCs (NPCs) in winter. Further, the magnitude of sensitivity of FIE (SIE) is low (high).
598 Also, the sensitivity of TIE is a linear sum of the sensitivities of FIE and SIE. Further, ACI
599 sensitivity values for PCs in summer are small, illustrating less dependency of CER on CDNC
600 in thick clouds.

601 The high (low) PR values are observed in summer (winter). Further, high PR values for
602 comparatively thin clouds with fewer $\text{CDNC} < \sim 50 \text{cm}^{-3}$ and intermediate for optically thick
603 clouds and $\text{CDNC} > \sim 50 \text{cm}^{-3}$ are observed. Sensitivity values are small (high) for thick clouds
604 in summer (winter).

605 Being one of the major source regions of anthropogenic aerosols across the globe, IGP
606 offers interesting insights into the study of ACPI coupled with aerosol indirect effects. This
607 study highlights that the aerosol-cloud relationship exhibits different behavior under
608 different meteorological conditions, at coastal and inland locations. Thus, compared to
609 other study areas, the stable atmospheric conditions due to the constant sea breeze
610 weakened the ACI over Karachi, which resulted in a smaller number of CDNC, NPCs, and
611 PCs. Further, our study also provides a very good platform for the detailed analysis of
612 sensitivity tests of aerosol indirect effects and precipitation formation.

613 Although the sample size limits the study, the observed trends offer important insights that
614 provide a foundation for future research. Therefore, further investigations with larger
615 sample sizes are suggested to validate and extend these findings.

616 **Limitations and future recommendations:**

617 Although the current study is as thorough as possible, however, it has its limitations due to
618 the topographical complexity of IGP, the lack of in-situ measuring instruments in Pakistan,
619 and the intrinsic uncertainties associated with satellite-based data. Therefore, simulations
620 of ground-based measurements along with satellite-based retrievals and calculation of
621 cloud properties and CCN by different Community Atmosphere Model (CAM) and
622 Weather Research and Forecasting (WRF) Models are recommended for deep insight into
623 the various mechanisms of ACPI over IGP.

624 **Data Availability:** The MODIS and TRMM data can be obtained from the NASA Goddard
625 Earth Sciences Data and Information Center (GES DISC) and can be retrieved from the
626 websites: <https://modis.gsfc.nasa.gov/data/> and <https://gpm.nasa.gov/data> . The reanalysis-
627 II datasets are obtained from the website:
628 <https://psl.noaa.gov/data/gridded/data.ncep.reanalysis2.html> . The processed datasets used
629 in this work are available on reasonable request from the corresponding author.

630 **Author contribution:** NG processed and analyzed the data and wrote the original draft of
631 the manuscript. KA proposed the Idea, supervised this work, and revised the manuscript.
632 YL helped in revising the manuscript.

633 **Acknowledgment:** The authors gratefully acknowledge the NASA Goddard Earth
634 Sciences Data and Information Services Center (GES DISC) for the provision of freely
635 available data retrieved from MODIS and TRMM. We are also grateful to the NOAA
636 Physical Sciences Laboratory (PSL) for free accessibility to (NCEP/NCAR) reanalysis-II
637 datasets.

638 **References**

639 Ackerman, A. S., Kirkpatrick, M. P., Stevens, D. E., & Toon, O. B.: The impact of humidity above stratiform
640 clouds on indirect aerosol climate forcing, *Nature.*, *432*, 1014-1017,
641 <https://doi.org/10.1038/nature03174> , 2004.

642 Alam, K., Iqbal, M. J., Blaschke, T., Qureshi, S., & Khan, G.: Monitoring spatio-temporal variations in aerosols
643 and aerosol–cloud interactions over Pakistan using MODIS data, *Adva. Space Res.*, *46*, 1162-1176,
644 <https://doi.org/10.1016/j.asr.2010.06.025>, 2010.

645 Alam, K., Qureshi, S., & Blaschke, T.: Monitoring spatio-temporal aerosol patterns over Pakistan based on
646 MODIS, TOMS and MISR satellite data and a HYSPLIT model, *Atmos. Envi.*, *45*, 4641-4651,
647 <https://doi.org/10.1016/j.atmosenv.2011.05.055>, 2011.

648 Albrecht, B. A.: Aerosols, cloud microphysics, and fractional cloudiness, *Sci.*, *245*, 1227-1230,
649 <https://doi.org/10.1126/science.245.4923.122> , 1989.

650 Ali, G., Bao, Y., Ullah, W., Ullah, S., Guan, Q., Liu, X., . . . Ma, J.: Spatiotemporal trends of aerosols over
651 urban regions in Pakistan and their possible links to meteorological parameters, *Atmo.*, *11*, 306,
652 <https://doi.org/10.3390/atmos11030306>, 2020.

653 Andreae, M., & Rosenfeld, D.: Aerosol–cloud–precipitation interactions. Part 1. The nature and sources of
654 cloud-active aerosols, *Earth. Sci. Rev.*, *89*, 13-41, <https://doi.org/10.1016/j.earscirev.2008.03.001>,
655 2008.

656 Anttila, T., Brus, D., Jaatinen, A., Hyvärinen, A. P., Kivekäs, N., Romakkaniemi, S., ... & Lihavainen, H.:
657 Relationships between particles, cloud condensation nuclei and cloud droplet activation during the third
658 Pallas Cloud Experiment, *Atmos. Chem. Phys.*, *12*, 11435-11450, [https://doi.org/10.5194/acp-12-11435-](https://doi.org/10.5194/acp-12-11435-2012)
659 [2012](https://doi.org/10.5194/acp-12-11435-2012) , 2012.

660 Anwar, K., Alam, K., Liu, Y., Huang, Z., Huang, J., & Liu, Y.: Analysis of aerosol cloud interactions with a
661 consistent signal of meteorology and other influencing parameters, *Atmos. Res.*, *275*, 106241,
662 <https://doi.org/10.1016/j.atmosres.2022.106241>, 2022.

663 Brenguier, J.-L., Pawlowska, H., Schüller, L., Preusker, R., Fischer, J., & Fouquart, Y.: Radiative properties of
664 boundary layer clouds: Droplet effective radius versus number concentration, *Atmos. Sci.*, *57*, 803-
665 821, [https://doi.org/10.1175/1520-0469\(2000\)057<0803:RPOBLC>2.0.CO;2](https://doi.org/10.1175/1520-0469(2000)057<0803:RPOBLC>2.0.CO;2) , 2000.

666 Chen, F., Sheng, S., Bao, Z., Wen, H., Hua, L., Paul, N. J., & Fu, Y. : Precipitation Clouds Delineation Scheme
667 in Tropical Cyclones and Its Validation Using Precipitation and Cloud Parameter Datasets from
668 TRMM, *Applied Met. Climatology.* *57*, 821-836, <https://doi.org/10.1175/JAMC-D-17-0157.1> , 2018.

669 Chen, Q., Yin, Y., Jin, L.-j., Xiao, H., & Zhu, S.: The effect of aerosol layers on convective cloud microphysics
670 and precipitation, *Atmos. Res.*, *101*, 327-340, <https://doi.org/10.1016/j.atmosres.2011.03.007>, 2011

671 Costantino, L., & Bréon, F.: Analysis of aerosol-cloud interaction from multi-sensor satellite observations,
672 *Atmos. Sci.*, *37*, <https://doi.org/10.1029/2009GL041828>, 2010

673 Fan, C., Ding, M., Wu, P., & Fan, Y.: The Relationship between Precipitation and Aerosol: Evidence from
674 Satellite Observation, *Atmos. Oce. Phy.*, <https://doi.org/10.48550/arXiv.1812.02036>, 2018.

675 Feingold, G., Eberhard, W. L., Veron, D. E., & Previdi, M.: First measurements of the Twomey indirect effect
676 using ground-based remote sensors, *Geophy. Res. Let.*, *30*, <https://doi.org/10.1029/2002GL016633>,
677 2003.

678 Gryspeerdt, E., Quaas, J., & Bellouin, N.: Constraining the aerosol influence on cloud fraction, *JGR. Atmos.*, *121*,
679 3566-3583, <https://doi.org/10.1002/2015JD023744> , 2016.

680 Guo, J., Su, T., Chen, D., Wang, J., Li, Z., Lv, Y., Zhai, P.: Declining summertime local-scale precipitation
681 frequency over China and the United States, 1981–2012: The disparate roles of
682 aerosols. *Geophy. Res. Letrs.*, *46*(22), 13281-13289, <https://doi.org/10.1029/2019GL085442> ,2019.

683 Hassan, M. A., Mehmood, T., Liu, J., Luo, X., Li, X., Tanveer, M., & Abid, M.: A review of particulate pollution
684 over Himalaya region: Characteristics and salient factors contributing ambient PM pollution. *Atmos.*
685 *Envi.*, *294*, 119472, <https://doi.org/10.1016/j.atmosenv.2022.119472> , 2022.

686 Hong, Y., Hsu, K. L., Moradkhani, H., & Sorooshian, S.: Uncertainty quantification of satellite precipitation
687 estimation and Monte Carlo assessment of the error propagation into hydrologic response, *Wat. Resc.*
688 *Res.*, *42*, 8, <https://doi.org/10.1029/2005WR004398> , 2006.

689 Hossain, F., Anagnostou, E. N., & Bagtzoglou, A.: On Latin Hypercube sampling for efficient uncertainty
690 estimation of satellite rainfall observations in flood prediction, *Comp. & geosc.*, *32*, 6, 776-792,
691 <https://doi.org/10.1016/j.cageo.2005.10.006> , 2006.

692 Houze Jr, R. A. Nimbostratus and the separation of convective and stratiform precipitation. In *International*
693 *geophysics.* Elsevier. 104, 141-163, 2014.

694

695 Jiang, H., Feingold, G., & Cotton, W.: Simulations of aerosol-cloud-dynamical feedbacks resulting from
696 entrainment of aerosol into the marine boundary layer during the Atlantic Stratocumulus Transition
697 Experiment, *JGR. Atmos.*, *107*, AAC 20-1-AAC 20-11, <https://doi.org/10.1029/2001JD001502>, 2002.

698 Jung, E.: Aerosol-cloud-precipitation interactions in the trade wind boundary layer, Ph.D Thesis, Meteorology
699 and Physical Oceanography, University of Miami, 91-pp., 2012.

700 Kang, N., Kumar, K. R., Yin, Y., Diao, Y., Yu, X.: Correlation analysis between AOD and cloud parameters to
701 study their relationship over China using MODIS data (2003-2013): impact on cloud formation and
702 climate change, *AAQR.*, *15*, 958-973, <https://doi.org/10.4209/aaqr.2014.08.0168>, 2015.

703 Kaskaoutis, D., Kumar Kharol, S., Sinha, P., Singh, R., Kambezidis, H., Rani Sharma, A.: Extremely large
704 anthropogenic-aerosol contribution to total aerosol load over the Bay of Bengal during winter season,
705 *Atmos. Chem. Phys.*, *11*, 7097-7117, <https://doi.org/10.5194/acp-11-7097-2011>, 2011.

706 Kedia, S., Ramachandran, S., Holben, B., & Tripathi, S.: Quantification of aerosol type, and sources of aerosols
707 over the Indo-Gangetic Plain, *Atmos. Envi.*, *98*, 607-
708 619, <https://doi.org/10.1016/j.atmosenv.2014.09.022>, 2014.

709 Koike, M., Asano, N., Nakamura, H., Sakai, S., Nagao, T., & Nakajima, T.: Modulations of aerosol impacts on
710 cloud microphysics induced by the warm Kuroshio Current under the East Asian winter monsoon, *JGR.*
711 *Atmos.*, *121*, 282-297, <https://doi.org/10.1002/2016JD025375>, 2016.

712 Koren, I., Kaufman, Y. J., Remer, L. A., & Martins, J. V.: Measurement of the effect of Amazon smoke on
713 inhibition of cloud formation. *Sci.*, *303*(5662), 1342-1345, <https://doi.org/10.1126/science.1089424>,
714 2004.

715 Kubar, T., Hartmann, D., & Wood, R.: Understanding the importance of microphysics and macrophysics for
716 warm rain in marine low clouds. Part I: Satellite observations, *Atmos. Sci.* *66*, 2953-2972,
717 <https://doi.org/10.1175/2009jas3071.1>, 2009.

718 Kumar, A., & Physics, S.: Variability of aerosol optical depth and cloud parameters over North Eastern regions
719 of India retrieved from MODIS satellite data, *Atmos. Sol. Terr. Phys.*, *100*, 34-
720 49, <https://doi.org/10.1016/j.jastp.2013.03.025>, 2013.

721 Kump, L. R., & Pollard, D.: Amplification of Cretaceous Warmth by Biological Cloud Feedbacks, *Sci.*, *320*,
722 195-195, <https://doi.org/10.1126/science.1153883>, 2008.

723 Li, J., Lv, Q., Zhang, M., Wang, T., Kawamoto, K., Chen, S., & Zhang, B.: Effects of atmospheric dynamics and
724 aerosols on the fraction of supercooled water clouds, *Atmos. Chem. Phys.*, *17*, 1847-
725 1863, <https://doi.org/10.5194/acp-17-1847-2017>, 2017.

726 López-Romero, J., Montávez, J., Jerez, S., Lorente-Plazas, R., Palacios-Peña, L., & Jiménez-Guerrero, P.:
727 Precipitation response to aerosol-radiation and aerosol-cloud interactions in regional climate
728 simulations over Europe. *Atmos. Chem. Phys.*, *21*, 415-430, <https://doi.org/10.5194/acp-21-415-2021>,
729 2021.

730 Masmoudi, M., Chaabane, M., Tanré, D., Gouloup, P., Blarel, L., & Elleuch, F.: Spatial and temporal variability
731 of aerosol: size distribution and optical properties, *Atmos. Res.*, *66*, 1-
732 19, [https://doi.org/10.1016/S0169-8095\(02\)00174-6](https://doi.org/10.1016/S0169-8095(02)00174-6), 2003.

733 McCoy, D., Field, P., Schmidt, A., Grosvenor, D., Bender, F., Shipway, B., & Elsaesser, G.: Aerosol midlatitude
734 cyclone indirect effects in observations and high-resolution simulations, *Atmos. Chem. Phys.*, *18*, 5821-
735 5846, <https://doi.org/10.5194/acp-18-5821-2018>, 2018.

736 Michibata, T., Kawamoto, K., & Takemura, T.: The effects of aerosols on water cloud microphysics and
737 macrophysics based on satellite observations over East Asia and the North Pacific, *Atmos. Chem. Phys.*,
738 *14*, 10515-10541, <https://doi.org/10.5194/acp-14-11935-2014>, 2014.

739 Myhre, G., Stordal, F., Johnsrud, M., Kaufman, Y., Rosenfeld, D., Storelvmo, T.: Aerosol-cloud interaction
740 inferred from MODIS satellite data and global aerosol models, *Atmos. Chem. Phys.*, *7*, 3081-3101,
741 <https://doi.org/10.5194/acp-7-3081-2007>, 2007.

742 Nair, V., Giorgi, F., Keshav Hasyagar, U.: Amplification of South Asian haze by water vapour-aerosol
743 interactions, *Atmos. Chem. Phys.*, *20*, 14457-14471, <https://doi.org/10.5194/acp-20-14457-2020>, 2020.

744 Naud, C., Posselt, D., & van den Heever, S.: Observed covariations of aerosol optical depth and cloud cover in
745 extratropical cyclones, *JGR: Atmos.*, *122*, 10-338, <https://doi.org/10.1002/2017JD027240>, 2017.

746 Rossow, W., & Schiffer, R.: Advances in understanding clouds from ISCCP, *Bul. Americ. Meteor. Soci.*, *80*,
747 2261-2288, [https://doi.org/10.1175/15200477\(1999\)080<2261:AIUCFI>2.0.CO;2](https://doi.org/10.1175/15200477(1999)080<2261:AIUCFI>2.0.CO;2), 1999.

748 Sharma, P., Ganguly, D., Sharma, A., Kant, S., Mishra, S.: Assessing the aerosols, clouds and their relationship
749 over the northern Bay of Bengal using a global climate model, *Earth. Spac. Sci.*, *10*, e2022EA002706,
750 <https://doi.org/10.1029/2022EA002706>, 2023.

751 Sherwood, S., Roca, R., Weckwerth, T., & Andronova, N.: Tropospheric water vapor, convection, and climate,
752 *Rev. of Geophy (AGU)*, *48*, 2, <https://doi.org/10.1029/2009RG000301>, 2010.

753 Singh, A., Rastogi, N., Sharma, D., Singh, D.: Inter and intra-annual variability in aerosol characteristics over
754 northwestern Indo-Gangetic Plain, AAQR., 15, 376-386, <https://doi.org/10.4209/aaqr.2014.04.0080>,
755 2015.

756 Srivastava, P., Pal, D., Aruche, K., Wani, S., & Sahrawat, K.: Soils of the Indo-Gangetic Plains: a pedogenic
757 response to landscape stability, climatic variability and anthropogenic activity during the Holocene,
758 Earth. Sci. Rev., 140, 54-71, <https://doi.org/10.1016/j.earscirev.2014.10.010>, 2015.

759 Stevens, B., & Feingold, G.: Untangling aerosol effects on clouds and precipitation in a buffered system,
760 Nature, 461, 607-613, <https://doi.org/10.1038/nature08281>, 2009.

761 Sun, J., & Ariya, P.: Atmospheric organic and bio-aerosols as cloud condensation nuclei (CCN): A review,
762 Atmos. Envi., 40, 795-820, <https://doi.org/10.1016/j.atmosenv.2005.05.052>, 2006.

763 Tao, W., Chen, J., Li, Z., Wang, C., & Zhang, C.: Impact of aerosols on convective clouds and precipitation,
764 Rev. Geophys., 50, <https://doi.org/10.1029/2011RG000369>, 2012.

765 Thomas, A., Kanawade, V., Sarangi, C., & Srivastava, A.: Effect of COVID-19 shutdown on aerosol direct
766 radiative forcing over the Indo-Gangetic Plain outflow region of the Bay of Bengal, Sci. Total Envi.,
767 782, 146918, <https://doi.org/10.1016/j.scitotenv.2021.146918>, 2021.

768 Tian, Y., & Peters-Lidard, C.: A global map of uncertainties in satellite-based precipitation
769 measurements, Geophys. Res. Let., 37, 24, <https://doi.org/10.1029/2010GL046008>, 2010.

770 Tripathi, S. N., Pattnaik, A., & Dey, S.: Aerosol indirect effect over Indo-Gangetic plain, Atmos. Envi., 41, 33,
771 7037-7047, <https://doi.org/10.1016/j.atmosenv.2007.05.007>, 2007.

772 Twomey, S.: The influence of pollution on the shortwave albedo of clouds, Atmos. Sci., 34, 1149-
773 1152, [https://doi.org/10.1175/1520-0469\(1977\)034<1149:TIOPOT>2.0.CO;2](https://doi.org/10.1175/1520-0469(1977)034<1149:TIOPOT>2.0.CO;2), 1977.

774 Verma, S., Ramana, M., & Kumar, R.: Atmospheric rivers fueling the intensification of fog and haze over Indo-
775 Gangetic Plains, Sci. Reports., Nature, 12, 5139, 2022.

776 Wang, F., Guo, J., Zhang, J., Huang, J., Min, M., Chen, T., Li, X.: Multi-sensor quantification of aerosol-induced
777 variability in warm clouds over eastern China. Atmos. Envi., 113, 1-9,
778 <https://doi.org/10.1016/j.atmosenv.2015.04.063>, 2015.

779 Wolf, E., & Toon, O.: Controls on the Archean climate system investigated with a global climate model,
780 Astrobiology, 14, 241-253, <https://doi.org/10.1089/ast.2013.1112>, 2014.

781 Wood, R.: Relationships between optical depth, liquid water path, droplet concentration, and effective radius in
782 adiabatic layer cloud, University of Washington, 3, 2006.

783 Wu, P., Dong, X., Xi, B., Liu, Y., Thieman, M., & Minnis, P.: Effects of environment forcing on marine
784 boundary layer cloud-drizzle processes, JGR: Atmos., 122, 4463-
785 4478, <https://doi.org/10.1002/2016JD026326>, 2017.

786 Wyant, M., Bretherton, C., Bacmeister, J., Kiehl, J., Held, I., Zhao, M., Soden, B.: A comparison of low-latitude
787 cloud properties and their response to climate change in three AGCMs sorted into regimes using mid-
788 tropospheric vertical velocity, Clim. Dyn., 27, 261-279, <https://doi.org/10.1007/s00382-006-0138-4>,
789 2006.

790 Yuan, T.: Increase of cloud droplet size with aerosol optical depth: An observation and modeling study, JGR: Atmos.,
791 113, D4, <https://doi.org/10.1029/2007JD008632>, 2008.

792 Yang, Y., Liu, X., Qu, Y., An, J., Jiang, R., Zhang, Y., & Ma, Q.: Characteristics and formation mechanism of
793 continuous hazes in China: a case study during the autumn of 2014 in the North China Plain. ACP, 15,
794 8165-8178, <https://doi.org/10.5194/acp-15-8165-2015>, 2015.

795 Zeb, B., Alam, K., Sorooshian, A., Chishtie, F., Ahmad, I., Bibi, H.: Temporal characteristics of aerosol optical
796 properties over the glacier region of northern Pakistan, Jour. Atmos. Sol-Terr. Phys., 186, 35-
797 46, <https://doi.org/10.1016/j.jastp.2019.02.004>, 2019.

798 Zhao, C., Tie, X., & Lin, Y.: A possible positive feedback of reduction of precipitation and increase in aerosols
799 over eastern central China, Geo. Res. Let., 33, 11, <https://doi.org/10.1029/2006GL025959>, 2006.

800 Zhou, S., Yang, J., Wang, W., Zhao, C., Gong, D., Shi, P.: An observational study of the effects of aerosols on
801 diurnal variation of heavy rainfall and associated clouds over Beijing-Tianjin-Hebei, Atmos. Chem.
802 Phy., 20, 5211-5229, <https://doi.org/10.5194/acp-20-5211-2020>, 2020.